

# **OPTIMAL RATE OF FREEZING BIOLOGICAL SYSTEMS**

A Thesis

Submitted to the Graduate Faculty of the  
Louisiana State University and  
Agricultural and Mechanical College  
In partial fulfillment of the  
requirements for the degree of  
Master of Science in Mechanical Engineering

in

The Department of Mechanical Engineering

By  
Sreedhar Thirumala  
B.Tech, J.N.T.U. College of Engineering  
J.N.T. University-2000  
May 2004

## **Acknowledgements**

It is a pleasure to thank the many people who made this thesis possible. First and foremost, I would like to thank my advisor, Dr. Ram V Devireddy, for lending his valuable time to teach and guide me, without whom this work would not have been possible. I would sincerely thank him for his technical insight and patience in motivating and nurturing me throughout this work. Next, I am grateful to my committee members, Dr. Charalampopoulos and Dr. Moldovan who have been helpful and generous with their time and expertise to evaluate my thesis.

I also thank all my friends and colleagues in the Bioengineering Laboratory, for providing me with an environment and support for my work. I extend my sincere gratitude to Venu Gopal Jogi for his valuable suggestions and for the fruitful discussions we had during my course and research work.

I am thankful to all my friends and well wishers, especially my roommates Muni Raju, Prashanth and Raghu, for their support in terms of providing congenial surroundings and making my stay at LSU memorable and enjoyable. I wish to specially thank my friends Keerthi, Deepika, Rekha and Sunil for helping me get through the difficult times, and for their support, amity and thoughts they provided which motivated towards my work.

There are countless other people whose names and faces pass through my mind as I ruminate about this period at LSU. So, I would have to include all of them saying that it was really a pleasure knowing them and that aspect, as much as anything else, made this whole journey worthwhile.

My final acknowledgement is due to my parents and family members back in India, who were always behind me with their prayers, love and blessings, encouraged me and provided tremendous support throughout my life. With out their help, I wouldn't have been here. I would like to dedicate this work to my beloved parents 'Saraswathamma' and 'Sada Nandam Thirumala'.

This research has been funded by a grant from Louisiana Board of Regents {LEQSF (2002-05)-RD-A-03}. I would like to thank them for their support.

# Table of Contents

ACKNOWLEDGEMENTS.....	ii
LIST OF TABLES.....	vi
LIST OF FIGURES.....	vii
NOMENCLATURE.....	ix
ABSTRACT .....	xi
CHAPTER 1. INTRODUCTION AND REVIEW.....	1
1.1 Cryobiology.....	1
1.2 Differential Scanning Calorimeter (DSC).....	4
1.3 Mathematical Model of Water Transport.....	11
1.4 Optimal Cooling Rate.....	14
1.5 Objectives of the Present Work.....	16
CHAPTER 2. A SIMPLIFIED PROCEDURE TO DETERMINE THE OPTIMAL RATE OF FREEZING BIOLOGICAL SYSTEMS.....	17
2.1 Introduction.....	17
2.2 Numerical Model and Simulations.....	19
2.2.1 Water Transport Model.....	19
2.2.2 Optimal Cooling Rate.....	19
2.2.3 Numerical Simulation.....	20
2.3 Results and Discussion.....	21
2.4 Conclusion. ....	35
CHAPTER 3. CRYOPRESERVATION OF CANINE SPERMATOZOA: THEORETICAL PREDICTION OF OPTIMAL COOLING RATES IN THE PRESENCE AND ABSENCE OF CRYOPROTECTIVE AGENTS.....	37
3.1 Introduction.....	37
3.2 Materials and Methods.....	40
3.2.1 Collection and Isolation of Sperm Cells.....	40
3.2.2 DSC Experiments.....	42
3.2.3 Translation of Heat Release to Cell Volume Data for Dynamic Cooling.....	42
3.3 Water Transport Model and Numerical Methods.....	44
3.3.1 Numerical Methods.....	46
3.4 Results.....	47
3.4.1 Dynamic Cooling Response and Membrane Permeability Parameters.....	47
3.4.2 Statistical Analysis.....	53
3.4.3 Combined Best-Fit Parameters.....	54
3.4.4 Water Transport Simulations.....	56

3.5 Discussion.....	60
3.5.1 Effect of Cooling Rate on Predicted Membrane Permeability Parameters.....	60
3.5.2 Experiments at Higher Cooling Rates.....	61
3.5.3 Parameter Sensitivity Analysis - Effect of Varying the Osmotically Inactive Cell Volume ( $V_b$ ).....	62
3.5.4 Effect of Extracellular Ice on Membrane Transport Parameters.....	66
3.5.5 Effect of CPA on Membrane Transport Parameters.....	68
3.5.6 Effect of CPAs on the Predicted Optimal Cooling Rates.....	69
3.6 Conclusion.....	70
REFERENCES.....	71
VITA.....	80

## List of Tables

Table 2.1: Physiologically Relevant Range of Model Parameters.....	18
Table 2.2: Linear Variation of Optimal Cooling Rate ( $B_{opt}$ , °C/min) with Reference Membrane Permeability ( $L_{pg}$ , $\mu\text{m}/\text{min}\cdot\text{atm}$ ).....	21
Table 2.3: Non-linear variation of Optimal Cooling Rate ( $B_{opt}$ , °C/min) with Activation Energy ( $E_{Lp}$ , Kcal/mole). ....	23
Table 2.4: Variation of Optimal Cooling Rate ( $B_{opt}$ ) with Diameter (D) and Inactive Cell Volume ( $V_b$ ).....	25
Table 2.5: Experimental vs. GOCRC Optimal Rates of Cooling.....	34
Table 3.1: Predicted Sub-Zero Membrane Permeability Parameters for Canine Sperm Cells in the Presence of Extracellular Ice.....	49
Table 3.2: Predicted Sub-Zero Membrane Permeability Parameters for Canine Sperm Cells in the Presence of Extracellular Ice and Glycerol.....	51
Table 3.3. Predicted Sub-Zero Membrane Permeability Parameters for Canine Sperm Cells in the Presence of Extracellular Ice and Dimethylsulfoxide ( $\text{Me}_2\text{SO}$ ).....	54
Table 3.4. Predicted Sub-Zero Membrane Permeability Parameters for Canine Sperm Cells in the Presence of Extracellular Ice and CPAs Assuming $V_b = 0.4V_o$ .....	64
Table 3.5. Predicted Sub-Zero Membrane Permeability Parameters for Canine Sperm Cells in the Presence of Extracellular Ice and CPAs Assuming $V_b = 0.8V_o$ .....	65

## List of Figures

Figure 1.1: DSC Experimental Arrangement.....	5
Figure 1.2: Schematic Representation of the DSC Control Loops.....	6
Figure 1.3: Typical DSC Curve.....	7
Figure 1.4: Superimposed Heat Flow Thermograms during Freezing of Osmotically Active (Curve A) and Inactive cells (Curve B).....	10
Figure 1.5: Inverse 'U' Curve. Effect of Cooling Rate on the Survival of a Representative Biological Cell .....	15
Figure 2.1 (A&B): The General Variation of the Predicted Optimal Cooling Rate ( $B_{opt}$ , °C/min) as a Function of Reference Permeability ( $L_{pg}$ , $\mu\text{m}/\text{min}\cdot\text{atm}$ ).....	22
Figure 2.2 (A&B): Plot of the Predicted Optimal Cooling Rate ( $B_{opt}$ , °C/min) as a Function of Activation Energy ( $E_{Lp}$ , Kcal/mole) with Error Bars Representing Positive and Negative Change in $E_{Lp}$ .....	24
Figure 2.3 (A&B): Variation of Optimal Cooling Rate ( $B_{opt}$ , °C/min) as a Function of Diameter, D (Fig. A) and Inactive Cell Volume, $V_b$ (Fig. B) at Different Criteria Based on Activation Energy ( $E_{Lp}$ ) of the Cell.....	26
Figure 2.4: The General Variation of the Predicted Optimal Cooling Rate ( $B_{opt}$ , °C/min) as a Function of End Temperature ( $T_{end}$ , °C) .....	28
Figure 2.5: Plot of the Predicted Optimal Cooling Rate ( $B_{opt}$ , °C/min) as a Function of Water Volume/Surface Area (SA/WV) .....	29
Figure 2.6: Generic Optimal Cooling Rate Chart (GOCRC).....	31
Figure 2.7: Generic Optimal Cooling Rate Chart (GOCRC). A Comparison of the GOCRC Predicted Optimal Cooling Rate Values and Experimentally Determined Values for a Variety of Biological Systems.....	33
Figure 3.1: Volumetric Response of Canine Sperm Cells as a Function of Subzero Temperatures Obtained Using the DSC Technique in the Presence of Extracellular Ice but in the Absence of CPAs.....	48
Figure 3.2(A-C): Volumetric Response of Canine Sperm Cells as a Function of Subzero Temperatures Obtained Using the DSC Technique in the Presence of Extracellular Ice and in the Presence of Glycerol as Cryoprotective Agent.....	50

Figure 3.3(A&B): Volumetric Response of Canine Sperm Cells as a Function of Subzero Temperatures Obtained Using the DSC Technique in the Presence of Extracellular Ice and in the Presence of Dimethylsulfoxide as Cryoprotective Agent.....52

Figure 3.4 (A-D): Contour Plots of the Goodness of Fit Parameter  $R^2$  (= 0.95) for Water Transport Response in Sperm Cells in Skim Milk Extender (Fig. A) and in Solutions with Glycerol as Cryoprotective Agent.....55

Figure 3.5 (A-F): Volumetric Response of Canine Sperm Cells at Various Cooling Rates as a Function of Subzero Temperatures Using the “Combined Best Fit” Membrane Permeability .....58

## Nomenclature

$L_{pg}$	Reference Membrane Permeability ( $\mu\text{m}/\text{min}\cdot\text{atm}$ )
$L_p$	Plasma Membrane Permeability ( $\mu\text{m}/\text{min}\cdot\text{atm}$ )
$E_{Lp}$	Activation Energy (Kcal/mole)
$B_{opt}$	Optimal Cooling Rate ( $^{\circ}\text{C}/\text{min}$ )
SA	Surface Area
WV	Initial Water Volume
$V_b$	Inactive Cell Volume
$V_o$	Isotonic or Initial Cell Volume
V	Cell Volume
$T_{\text{end}}$	End Temperature at which Water Transport Ceases
T	Absolute Temperature (K)
$T_r$	Reference Temperature (273.15K)
$\%W_T$	% of Water Trapped Inside the Cell
$A_c$	Effective Membrane Surface Area Available for Water Transport
$v_w$	Molar Volume of Water ( $18 \times 10^{12} \mu\text{m}^3/\text{mole}$ )
$a_w^o$	Chemical Potential of Extracellular Fluid
$a_w^i$	Chemical Potential of Intracellular Fluid
R	Gas Constant ( $8.02 \times 10^{13} \mu\text{m}^3\cdot\text{atm}/\text{mol K}$ )
$\Delta H_f$	Latent Heat of Fusion of Water (335 J/gm)
$C_i$	Initial Cell Osmolality (0.285)
$\Delta q_{dsc}$	Measured Difference in Heat DSC Release (mJ/mg total sample)
DSC	Differential Scanning Calorimeter

$\varphi_s$	Dissociation Constant for <i>NaCl</i> (=2)
$n_s$	Number of Moles of Solutes in the Cell ( $C_i (V_o - V_b)$ )
$\Delta X$	Distance Between Sinusoids ( $\mu\text{m}$ )
$r_v$	Vascular Radius ( $\mu\text{m}$ )
$L$	Axial Length of Krogh Cylinder ( $\mu\text{m}$ )
<i>GOCRC</i>	Generic Optimal Cooling Rate Chart
<i>GOCRE</i>	Generic Optimal Cooling Rate Equation
$B_{\text{GOCRC}}$	Cooling Rate on Y-axis of <i>GOCRC</i>
$\Delta q(T)_{dsc}$	Fractional Heat Release Difference During Initial and Final Cooling Runs
$L_{pg}[CPA]$	Reference Membrane Permeability in Presence of CPA ( $\mu\text{m}/\text{min-atm}$ )
$E_{Lp}[CPA]$	Activation Energy in Presence of CPA (Kcal/mole)
$\chi^2$	Residual Variance
<i>CBF</i>	Combined Best Fit
$\rho$	Density of Water ( $1000 \text{ kg}/\text{m}^3$ )

## Abstract

This thesis addresses optimization techniques for cryopreservation of biological systems. A part of the thesis (Chapter 2) reports a simplified procedure to predict the optimal rate of freezing biological systems once the cell level parameters are known *a priori*. The key cell level parameters investigated were, reference permeability of the membrane to water ( $L_{pg}$ ), apparent activation energy ( $E_{Lp}$ ), inactive cell volume ( $V_b$ ), diameter ( $D$ ), and the ratio of the available surface area for water transport to the initial volume of intracellular water ( $SA/WV$ ). The simplified procedure was developed by performing a thorough analysis of the water transport model over a physiologically relevant range for the various cell level parameters. The results from the parametric analysis are analyzed and used to develop a Generic Optimal Cooling Rate Chart (GOCRC) and a Generic Optimal Cooling Rate Equation (GOCRE). The use of GOCRC and GOCRE greatly simplifies the prediction of the optimal rate of freezing of biological systems without resorting to complex numerical simulations. The second and last part of the thesis (Chapter 3) reports the membrane permeability parameters ( $L_{pg}$  and  $E_{Lp}$ ) of canine sperm cells during freezing using a differential scanning calorimeter (DSC) technique. In this study a well established shape independent Differential Scanning Calorimeter (DSC) technique was used to measure the dehydration response during freezing of ejaculated canine sperm cells. Volumetric shrinkage during freezing of canine sperm cell suspensions was obtained at cooling rates of 5 and 10 °C/min in the presence of extracellular ice and with or without cryoprotective agents (CPAs). By fitting a model of water transport to the experimentally obtained volumetric shrinkage data the best fit membrane permeability parameters ( $L_{pg}$  and  $E_{Lp}$ ) were determined. Numerical

simulations of water transport in canine sperm cells were then performed under a variety of cooling rates (5 to 100 °C/min) using the experimentally determined membrane permeability parameters ( $L_{pg}$  and  $E_{Lp}$ ). The simulation results were analyzed to predict the amount of water left in the cell after dehydration ceased, in the absence of IIF and the “optimal cooling rates” for canine sperm cryopreservation.

# Chapter 1

## Introduction & Review

### 1.1 Cryobiology

Cryobiology is that branch of science, which deals with the effects of reduced temperatures on living organisms, their constituent parts, and their products. One important goal of the field of cryobiology is to preserve and store viable biological systems in the frozen state for extended periods of time in order to ensure reproducible results and continuity in research and biomedical processes. One such technique to preserve and genetically stabilize the biological systems is the “cryopreservation” process. Cryopreservation refers to the storage of a living organism at ultra- low-temperature in suspended animation for longer periods of time, such that it can be revived and restored to the same living state as before it was stored. Advances in cryopreservation technology have made it possible to develop new methods that allow low temperature maintenance of a variety of cell and tissue systems. Cryopreservation techniques are developed for the preservation of various biological systems such as, microorganisms, isolated tissue cells, small multicellular organisms and even more complex organisms such as embryos. These techniques have been successfully applied to a variety of mammalian systems such as red blood cells, lymphocytes, platelets, granulocytes, gametes and embryos, hepatocytes, bone marrow stem cells, cornea and skin, pancreatic tissue, heart and kidney, etc. as reviewed by Mazur (1984) and McGrath (1975). Other viewpoints of applied cryobiology that are of significance include the preservation of human and non-human mammalian oocytes (Bernard and Fuller 1996), food freezing, tissue engineered equivalents (Oegema *et al* 1999), protozoa and parasites, insects, fish, microorganisms and plants, including algae (Walsh). Other applications

include cryopreservation of rat and human liver slices (Day *et al* 1999), fish gametes and aquatic species and spermatozoa from variety of species, including human sperm (Devireddy *et al* 1998, Devireddy *et al* 2002).

The freezing process involves complex phenomenon that, even after decades of research, are not fully understood. Water is the major component of all living cells and it must be available for all the chemical processes of life to occur and cellular metabolism stops when all the water in the system is converted to ice. As the cell water is considered essential to the structure and efficient functioning of living cells, therefore, the state of the water plays a vital role in cell survival during a freezing process. It's important to understand, qualitatively and quantitatively, what happens to this cell water as the cells are subjected to freezing temperatures. Ice tends to form at different rates during a freezing process. As the cell in solution is subjected to a freezing protocol, ice first forms in the extracellular space. The cell membrane prevents the formation of ice inside the cell and as a result the intracellular solution becomes super cooled. Due to the fact that the partially frozen extracellular solution has a lower chemical potential than the unfrozen super cooled intracellular solution, a chemical potential difference is established across the cell membrane (Mazur 1970). This results in a thermodynamically non-equilibrium state that provides a driving force for the two biophysical processes during freezing, cellular dehydration or the loss of intracellular water and the formation of intracellular ice (Mazur 1984). At low cooling rates cellular dehydration is the dominant mechanism while at very rapid cooling rates intracellular ice formation (IIF) is the dominant mechanism (Mazur 1963). Both cellular dehydration and IIF have been shown to be deleterious to the post-thaw survival of biological systems (Lovelock 1953; Mazur *et al* 1972). The rate of cooling has a dramatic effect on these two biophysical processes. If the cooling velocity is sufficiently slow, there will be sufficient

time for the cell water to leave the cell and join the extracellular space. The result is the cell loses water rapidly by exmosis to concentrate the intracellular liquid sufficiently enough to eliminate super cooling and maintain chemical potential of intracellular water in equilibrium with that of extracellular water. The resulting changes in the extracellular region, such as changes in pH, changes in ionic concentration cause the tertiary structure of proteins to unfold, so that some of its original properties, especially its biological activity, are diminished or eliminated. This denaturation of cell proteins may be lethal to cell survival (Lovelock 1953). In addition, mechanical interaction between extracellular ice crystals and cells can also lead to the deformation of cells and rupture of cell membranes (Ishiguro and Rubinsky 1994). On the other hand if the cell is cooled too rapidly it is not able to lose water fast enough to reach equilibrium; it becomes increasingly super cooled and eventually attains equilibrium by freezing intracellularly. Intracellular ice formation (IIF) is generally lethal as it causes injury to cellular membranes and intracellular structures. So, cooling rates which are either “too slow” or “too fast” can and do reduce the post thaw survival of the cells, therefore, a cooling rate for maximum cell cryosurvival should and does exist between the "high" and "low" rates (McGrath 1988). This has been confirmed experimentally for a variety of cells and the curve of cell survival plotted as a function of the cooling rate, has a characteristic U-shape (Mazur *et al* 1972). Permeability of the membrane shows how fast the water can leave the cell at a given cooling rate. More the permeability of the membrane, more the water transport across the cell membrane in a given time and vice versa. Therefore, whether a prescribed cooling rate is too “slow ” or too “fast,” is a function of cell membrane permeability to water and the probability that any water remaining trapped within the cell at any given subzero temperature will nucleate and turn to ice. The difference in membrane permeability to water and probability of IIF results in different optimal

cooling rates for different cells. Therefore, to find out the optimal cooling rate for maximum cell survival and to optimize a cryopreservation protocol, it is important to measure the cell membrane's permeability to water. Clearly, the quantitative understanding of the water transport across the cell membrane during a cryopreservation is critical for the success of the respective protocol.

Water transport during freezing has been extensively studied by using various methods. One such method is measurement of water transport in single spherical cells by using cryomicroscopy technique (Cosman *et al* 1989; Diller and Cravalho 1970; McGrath 1988). Cryomicroscopy involves the application of cryogenic temperatures to cellular systems mounted under a light microscope to study the biophysical response of cells to freezing. The quantitative measurement of water transport during freezing of a tissue system were efficiently performed by using directional solidification device and two-step freezing technique (Pazhayannur and Bischof 1997). A shape independent Differential Scanning Calorimeter (DSC) technique has recently been applied to measure the membrane permeability parameters in both cell and tissue systems (Devireddy *et al* 1998, Devireddy *et al* 2002(b)).

## **1.2 Differential Scanning Calorimeter (DSC)**

Whenever a material undergoes a change in physical state, heat is either liberated or absorbed. Many physical changes such as melting, solidifying or changing from one crystalline form to another are simply initiated by raising or dropping the temperature of the material. Differential Scanning Calorimeter is primarily used to measure energy changes with respect to changes in temperature. Specific quantities measured are phase change enthalpies, reaction kinetics, heat capacities, glass transition temperatures, thermal history, decomposition effects, and the purity of solid samples (McNaughton and Mortimer 1975). The two main types of DSC

instruments are the power compensated and heat flux, both measures heat applied, but power compensated holds the temperature to a preset value while the heat flux holds the heat applied constant.

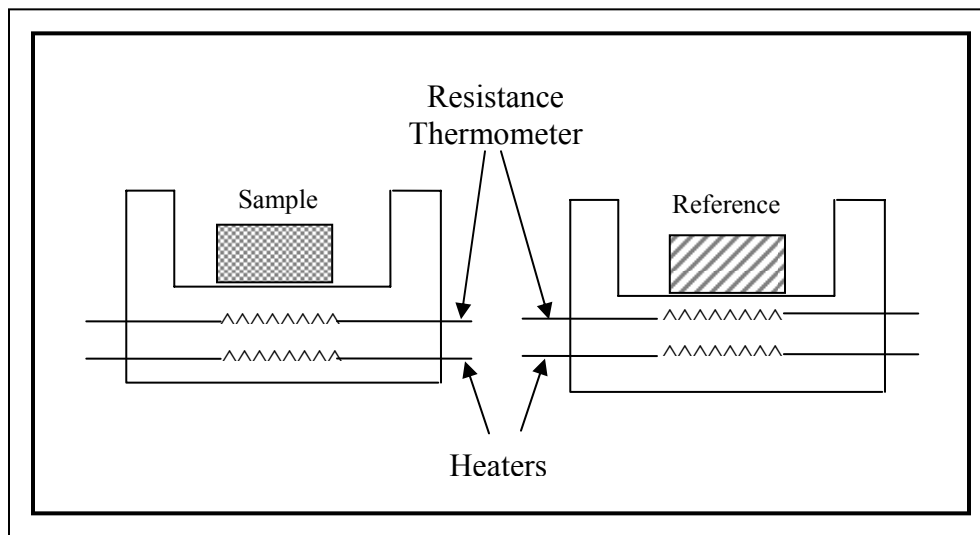


Figure 1.1: DSC experimental

The DSC, which we used for our experiments, is the Perkin-Elmer DSC 7, which is a power compensated model and can run from  $-170$  to  $725$  °C. In power compensation method the DSC measures the amount of power required to keep the sample at the temperature predetermined by the program. The heat flow to keep a reference (empty sample container) at the same temperature is also measured, and the heat reading is the difference between the sample and reference.

The experimental setup for the DSC is shown in Fig 1.1. The DSC basically consists of a sample holder and a reference holder, which are insulated from each other. The sample is placed inside the sample holder and reference holder is usually kept empty. Individual heaters are provided for both sample and reference holders through which heat power is supplied.

Thermometers are used to measure the temperatures throughout the process. The sample and reference holder are always maintained at the same temperature by means of two control loops as shown in Fig 1.2 (redrawn from: McNaughton and Mortimer 1975)

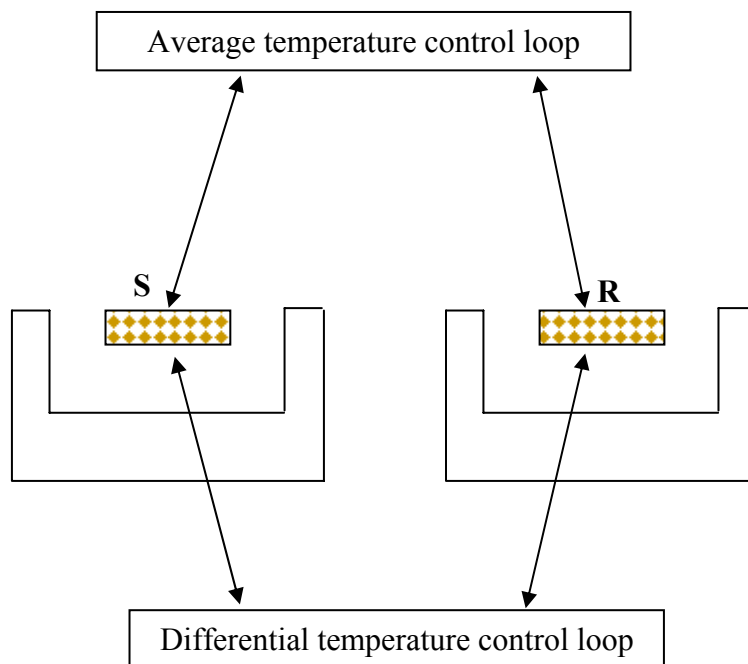


Figure 1.2: Schematic representation of the DSC control

The average temperature control loop changes the temperature of sample and reference at a constant programmed rate set by the user. As the reference sample (R) is an empty sample holder, a temperature difference should occur due to the exothermic or endothermic reactions in the sample (S). The differential temperature control loop eliminates this difference by automatically adjusting the power input to the heater circuit. This is the ‘null balance’ principle. Thus the temperature of the sample holder is kept at the same temperature of the reference holder by continuous and automatic adjustment of the heater power. A signal proportional to the

difference between the heat input to the sample and that to the reference,  $dH/dT$ , is fed into a recorder and plotted as a function of temperature.

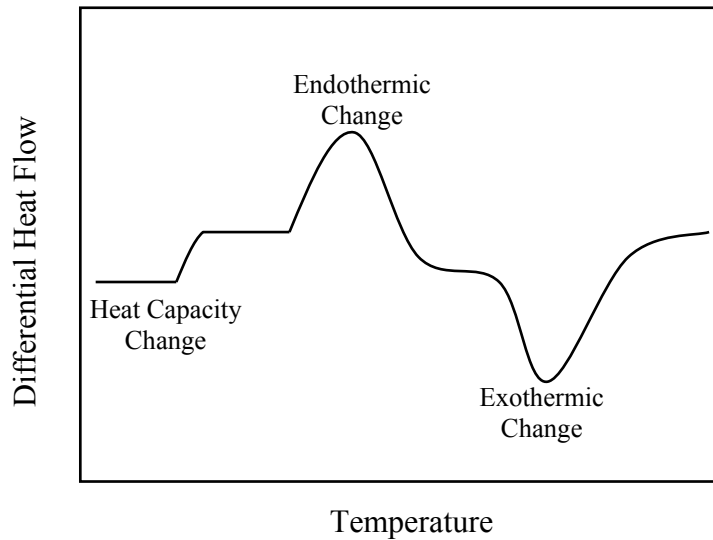


Figure 1.3: Typical DSC

A typical example of the DSC curve is shown in Fig 1.3. As the temperature increases at a set rate, the evolution or absorption of heat by a sample and change in enthalpy during a phase change process can be measured by calculating the area under peaks that occur in the heat flow versus time or heat flow versus temperature graphs. Also from the peaks generated by a phase transition, we can calculate the melting point fairly accurately by finding the onset temperature. Onset temperature is defined as the intercept between the baseline and a line drawn tangent to leading edge of the curve, near the apex. The area under the peaks is calculated from the baseline created by the heat capacity of the substance. The difference in heat capacities of the sample and reference causes the experimental curve to shift along the ordinate axis by a constant value or one barely changing with temperature and also causes the base line to shift from the zero level. This problem can be eliminated by using a reference with a heat capacity very close to heat capacity of the sample being studied. Generally an empty pan of the same material as the

sample pan is used as the reference pan to reduce the heat capacity differences (Gray 1976). The output signal, which is directly proportional to the differential heating power, would directly stand for the heat flow rate into the sample. This is obtained only when all the electric energy is converted into heat energy and is transferred to the sample or reference. For this purpose the thermal resistances should be reduced as much as possible by keeping the thermal mass of the sample to a minimum. Also, there must be a negligible heat loss due to the thermal resistance between the sample and sample pan and similarly, between the sample pan and sample holder. This is achieved by using small masses of the sample and by calibration.

To ensure the accuracy and repeatability of the experimental data, the limitations of the DSC machine should be studied and a set of calibration and control experiments must be performed (Devireddy *et al* 1998). These include (a) calibration of the machine and minimization of the thermal lag: The temperature scale of the instrument must be calibrated by the melting point of pure ice (273.15 K or 0 °C). The transition enthalpies are based on the heat of fusion of pure ice (335 J/g). All calibrations must be checked and if necessary corrected several times during the course of the experiments; (b) minimization of the thermal gradients within the sample by using low sample sizes: It is found that thermal lag is proportional to the mass of the sample and the scan rate. Therefore, a low and evenly distributed sample mass (10-15mg) and a low scan rate ( $\leq 20$  °C/min) must be used; (c) minimization of the baseline error by selection of sigmoidal base line for phase change during freezing: As DSC measures heat flow, not heat, the area under the heat flow vs. time (or temperature) curve is the measurement of interest. This area must be determined with respect to a reference or a base line. As the differences in the specific heat capacity between water and ice causes a shift in the base line of the thermogram, it is necessary to use a nonlinear (in our case sigmoidal) baseline to measure the area under the

thermogram more accurately. The baseline can be estimated by drawing tangents at assumed initial and final points on the thermogram. The DSC software will be used to draw a sigmoidal baseline between the two tangents, which is then used as a reference to measure the heat liberated during that event (Devireddy *et al* 1998); (d) condensation effects: At subzero temperature there is a possibility of condensation of the air both inside and outside of the sample pan as well as in the chamber surrounding the pan. The resulting heat release will lead to an incorrect reading of the heat released during solidification of the sample. The condensation outside of the sample is assumed to be negligible, since dry helium gas will be used to purge the condensable water-laden room air from the DSC head. For condensation inside the sample pan, an analysis showed that the amount of heat release expected from the condensation of saturated water vapor of the same volume held inside the sample pan as held inside the DSC pan at 5 °C would account for less than 0.5% of the heat release measured in a typical experiment. Hence, it is argued that the effects of condensation are assumed to be negligible in DSC experimental setup (Devireddy *et al* 1998); (g) error due to the ice nucleant *P. syringae* in heat release measurements: In DSC experiments 0.5-1.0 mg of *Pseudomonas syringae* is always added to the cell suspension in order to nucleate the extracellular space  $\geq -4$  °C in all samples. The effect *P. syringae* can be neglected in the water transport analysis as the DSC heat release readings were found to be identical ( $\pm 2\%$ ) in both the cases (DSC experiments with and without *P. syringae*) per milligram of media (Devireddy *et al* 1998); (h) error due to noise in the DSC readings: It is found that the error due to the noise is very small and it can be neglected during DSC experiments (Devireddy *et al* 1998).

Devireddy *et al* (1998) effectively used DSC technique to obtain dynamic and quantitative water transport data in cell suspensions during freezing. The method is based on the

fact that heat release of a pre-nucleated sample containing osmotically active cells in media is always greater than the final heat release of an identical sample of osmotically inactive or lysed cells in the same media.

Fig 1.4 shows the heat flow thermograms during freezing of osmotically active cells,  $q_{initial}$  (curve A) and osmotically inactive cells,  $q_{final}$  (curve B). The area of the curve A under a given base line is greater than the area of the curve B, representing heat release during freezing of live

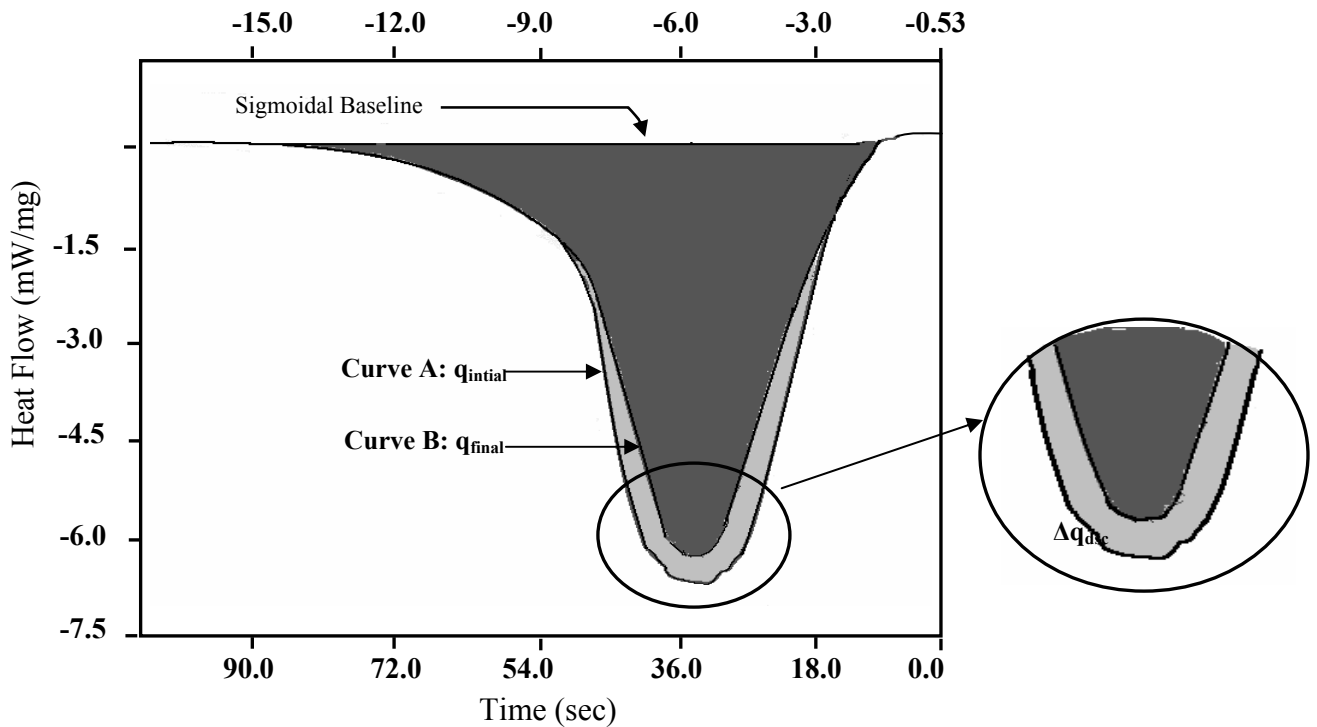


Figure 1.4: superimposed heat flow thermograms during freezing of osmotically active (Curve A) and inactive cells (Curve B)

cells is more than the heat release during freezing of lysed or dead cells. The heat release measurements of interest are  $\Delta q_{dsc}$  and  $\Delta q(T)_{dsc}$  which are the total and fractional difference between  $q_{initial}$  and  $q_{final}$ . This difference in heat release has been shown to be related to cell

volume changes by using the following mathematical formula,

$$\frac{V_o - V(T)}{V_o - V_b} = \frac{\Delta q(T)_{dsc}}{\Delta q_{dsc}} \quad (1.1)$$

We can rearrange this equation to measure water transport data from the DSC measured heat releases  $\Delta q(T)_{dsc}$  and  $\Delta q_{dsc}$  as,

$$V(T) = V_o - \frac{\Delta q(T)_{dsc}}{\Delta q_{dsc}} \cdot (V_o - V_b). \quad (1.2)$$

The unknown  $V_o$  is the initial or isotonic cell volume and  $V_b$  is the osmotically inactive cell volume. The detailed description and various assumptions made in deriving the above equations are given elsewhere (Devireddy *et al* 1998).  $V_o$  &  $V_b$  are to be obtained using correlative microscopy techniques as described elsewhere (Cosman *et al* 1989; Pazhayannur and Bischof 1997). Equation (1.2) can be used to generate cell volume changes from the experimentally measured DSC heat release data in the subsequent analysis, which is explained in chapter 3. Equation (1.2) is verified in the results by comparison to cryomicroscopy data for the identical freezing conditions (Devireddy *et al* 1998).

### 1.3 Mathematical Model of Water Transport

A mathematical model has been developed by Mazur (1963) for predicting the volumetric change in cells due to the loss of intracellular water across the cell membrane during a freezing process in the presence of extra cellular ice. Mazur's water transport model was later modified by Levin *et al* (1976), by presuming the permeability of the membrane depends on the temperature. Water transport model assumes an idealized biological cell as an open thermodynamic system having a semi-permeable membrane boundary. The model also assumes: 1) infinite extracellular space while the cellular space is the volume of sphere ( $V= 4\pi r^3/3$ ); 2) the

cellular space is the volume of the geometry of the cell being studied; 3) effective membrane surface area available for water transport ( $A_c = 4\pi r_o^2$ ) is constant based on the original cell radius,  $r_o$  (Leibo 1980; Toner *et al* 1991); 4) the intracellular solution is ideal and dilute (Mansoori 1975; Levin 1977); 5) the temperature differentials across the cell membrane are negligible; and 6) the latent heat of water is constant (335 mJ/mg) in the temperature range of interest (Mazur 1963); 6) the hydrostatic pressure difference across the cell plasma membrane is zero (a good assumption for mammalian cells). The plasma membrane permeability is assumed to be temperature dependent and is represented by an Arrhenius relationship as given by Levin *et al* (1976) and shown in Eq. 1. 9. In its simplest form water transport model can be represented as,

$$\frac{dV}{dT} = - \frac{L_p A_c R T}{B v_w} \left( \ln \frac{a_i^w}{a_o^w} \right) \quad (1.3)$$

where  $V$  is the cell volume,  $T$  is the absolute temperature,  $L_p$  is the permeability of the membrane to water,  $R$  is the gas constant,  $B$  is the constant cooling rate,  $A_c$  is the effective membrane surface area available for water transport,  $v_w$  is the partial molar volume of water, and  $a_i^w$  is the chemical potential of the intracellular fluid and  $a_o^w$  is the chemical potential of extracellular fluid. Quantitative use of the above thermodynamic model requires a more complete specification of the chemical activities of the extracellular and the intracellular solutions, along with the membrane water permeability.

The extracellular solution is assumed to be composed of a binary solution consisting of water and sodium chloride and can be modeled using the equilibrium properties of a solid/liquid

solution. The Gibbs-Helmholtz equation relates the equilibrium water activity in the solution as a function of temperature as,

$$\frac{\partial(\ln a_w)}{\partial T} = \frac{\Delta H_f}{RT^2} \quad (1.4)$$

where  $\Delta H_f$  is the latent heat of fusion of water, which is assumed to be constant in the temperature range of interest (0 to  $-45$  °C) as 335 mJ/mg. Integrating the above expression yields the extracellular activity as,

$$\ln a_w = \frac{\Delta H_f}{R} \left[ \frac{1}{T_R} - \frac{1}{T} \right] \quad (1.5)$$

where  $T_R$  is the reference temperature (273.15 K). The intracellular solution is typically modeled as an ideal and dilute solution so that the chemical activity of the internal water is equal to the mole fraction of the water,

$$a_w^i = X_w^i \quad (1.6)$$

Neglecting the cell membrane volume and recognizing that some of the intracellular fluid may be bound water, that is water which is not free to move across the cell membrane in response to an osmotic gradient (which is included in the osmotically inactive cell volume  $V_b$ ), the mole fraction of intracellular water is given as,

$$X_w^i = \frac{V - V_b}{(V - V_b) + \phi_s n_s \nu_w} \quad (1.7)$$

where  $\phi_s$  is the disassociation constant for sodium chloride,  $n_s$  is the number of moles of solutes in the cell as calculated from initial cell osmolarity and the total osmotically active cell water volume ( $V_o - V_b$ ) where  $V_o$  is the initial isotonic cell volume and,  $V_b$  is the osmotically inactive cell volume. Substituting Eqs. 1.5 and 1.7 in Eq. 1.3, one arrives at the Mazur model of water transport,

$$\frac{dV}{dT} = -\frac{L_p A R T}{B v_w} \left[ \ln \left( \frac{(V - V_b)}{(V - V_b) + v_w (v_s \phi_s)} \right) - \left( \frac{\Delta H_f}{R} \left[ \frac{1}{T_R} - \frac{1}{T} \right] \right) \right] \quad (1.8)$$

The temperature dependence of the membrane permeability to water ( $L_p$ ) is expressed as an Arrhenius relationship (Levin *et al* 1976),

$$L_p = L_{pg} \exp \left[ -\frac{E_{Lp}}{R} \left( \frac{1}{T} - \frac{1}{T_R} \right) \right] \quad (1.9)$$

where  $L_{pg}$  is the permeability of the membrane to water at a reference temperature ( $T_R = 273.15$  K) and  $E_{Lp}$  is the apparent activation energy for the permeability process.

#### 1.4 Optimal Cooling Rate

As stated earlier, cooling rate either “too high” or “too low” can reduce the post thaw survival of the cells either by “intracellular ice formation” or by “solute damage” respectively. Based upon this, a cooling rate for maximum cell cryosurvival should exist between the "high" and "low" rates which is referred as optimal cooling rate for a given cell type. This has been confirmed experimentally for a variety of cells and the curve of cell survival plotted as a function of the cooling rate, has a characteristic U-shape (Fig 1.5).

Fig 1.5 shows a representative survival curve for a cell type as a function of cooling rate. In Fig 1.5 the survival fraction progressively increases with increasing cooling rate as solute effects are minimized. Survival reaches a maximum which presumably just precedes the first appearance of IIF, following which viability falls as the proportion of cells with IIF increases. Since the extent

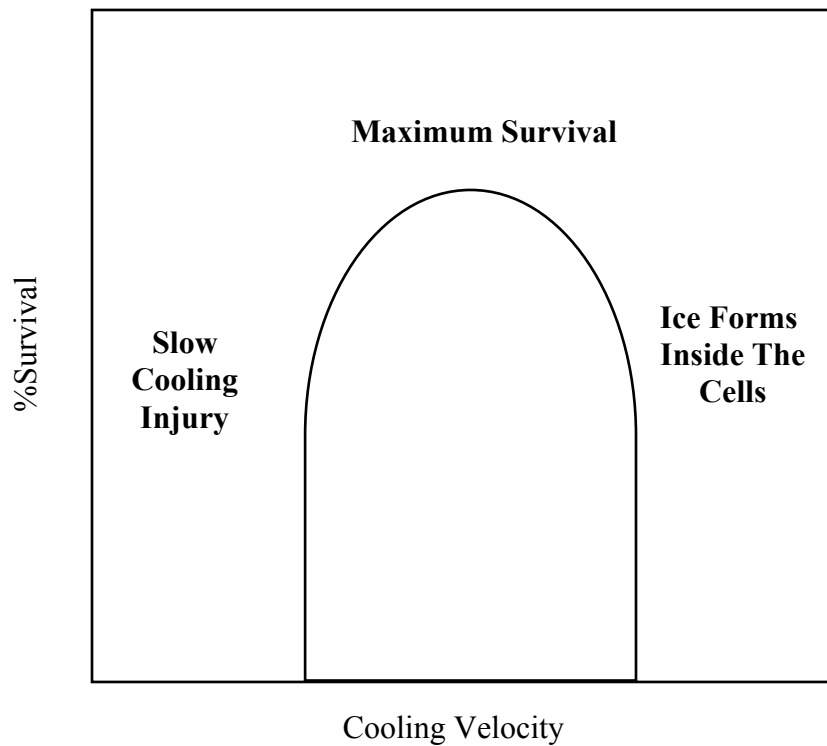


Figure1.5 Inverse 'U' Curve. Effect of cooling rate on the survival of a representative biological cell

and nature of ice formation is critical to the success of the freezing protocol , precise quantitative information about the rate and amount of water transport out of the cells at subzero temperatures is necessary.

## 1.5 Objectives of the Present Work

The objectives of the present work are as follows.

- Understand the damage caused by the freezing process during a cryopreservation protocol.
- Study the effect of several cell level parameters on the predicted optimal cooling rate of an arbitrary biological system by using a well defined water transport model and develop a simplified method of calculating optimal cooling rate of any biological system without resorting to any numerical simulations.
- To obtain the water transport data of canine sperm cells in the presence of extracellular ice and cryoprotective agents (CPAs) during freezing by using a widely accepted DSC technique at different cooling rates.
- Use the data obtained from the DSC experiments and to predict the membrane permeability parameters by curve fitting the DSC data to a water transport model.

## Chapter 2

### A Simplified Procedure to Determine the Optimal Rate of Freezing Biological Systems

#### 2.1 Introduction

As explained in the main introduction part of the thesis, freezing usually occurs outside the cell first, because that's where there are more freezing nuclei and because of the membrane properties which does not allow the ice formation inside the cell. When this happens, the extracellular solutes are concentrated in a small quantity of unfrozen water, which necessarily has a higher chemical potential compared to the intracellular super cooled solution. This chemical potential difference causes water to leave the cell and creates a thermodynamically non-equilibrium state that provides a driving force for the two biophysical processes during freezing, cellular dehydration and the formation of intracellular ice (Mazur 1984). At low cooling rates cellular dehydration is the dominant mechanism while at very rapid cooling rates intracellular ice formation (IIF) is the dominant mechanism (Mazur 1963). Both cellular dehydration and IIF have been shown to be deleterious to the post-thaw survival of biological systems (Mazur 1972, Lovelock 1953). Thus, biophysical optimization of cryopreservation process demands precise information about the rate and amount of water transport out of the cells at subzero temperatures. Based on a model of water transport by Mazur (Mazur 1963), the loss of intracellular water is dependent on various cell level parameters: permeability of the membrane to water ( $L_{pg}$ ), apparent activation energy ( $E_{Lp}$ ), inactive cell volume ( $V_b$ ), diameter ( $D$ ), end temperature at which water transport is assumed to cease ( $T_{end}$ ), and the ratio of the available surface area for water transport to the initial volume of intracellular water ( $SA/WV$ ).

This study reports a simplified procedure to predict the optimal rate of freezing biological systems once the cell level parameters ( $L_{pg}$ ,  $E_{Lp}$ , and SA/WV) are known *a priori*. The simplified procedure was developed by performing a thorough analysis of the water transport model over a physiologically relevant range for the various cell level parameters. The key cell level parameters

Table 2.1: Physiologically Relevant Range of Model Parameters

<b>Parameter</b>	<b>Range Selected</b>	<b>Step Size</b>
$L_{pg}$	0.01 to 100.00 $\mu\text{m}/\text{min-atm}$	10.0 $\mu\text{m}/\text{min-atm}$
$E_{Lp}$	4.0 to 100.00 Kcal/mole	2.0 Kcal/mole
$V_b$	0.1 $V_o$ to 0.9 $V_o$	0.1 $V_o$
$T_{\text{end}}$	-45 °C to -15 °C	-15 °C
D	5.0 to 100.0 $\mu\text{m}$	5.0 $\mu\text{m}$

investigated were,  $L_{pg}$ ,  $E_{Lp}$ ,  $V_b$ , D, and SA/WV. The results from the parametric analysis are analyzed to establish a new and simpler procedure to calculate the predicted optimal cooling rates for an arbitrary biological system without resorting to complex numerical simulations. Optimal cooling rate ( $B_{\text{opt}}$ ) is determined assuming a damaging criterion for initial percentage of water trapped ( $\%W_T$ ), along with the end temperature at which water transport is assumed to cease ( $T_{\text{end}}$ ). In this study  $B_{\text{opt}}$  is defined as the “highest” cooling rate at which 5% of the initial water volume is trapped inside the cell at an assumed end temperature of -15 °C. For each parameter a physiologically relevant range is selected (see Table 2.1).

## 2.2 Numerical Model and Simulations

### 2.2.1 Water Transport Model

Mazur (1963) developed a mathematical model for the volumetric change in cells due to the water transport during freezing process in the presence of extracellular ice. The reduction in cellular volume due to the water transport across the cell membrane was modeled thermodynamically as (Eqn.1.8),

$$\frac{dV}{dT} = -\frac{L_p ART}{B v_w} \left[ \ln \left( \frac{(V - V_b)}{(V - V_b) + v_w (v_s \phi_s)} \right) - \left( \frac{\Delta H_f}{R} \left[ \frac{1}{T_R} - \frac{1}{T} \right] \right) \right]$$

with  $L_p$ , the plasma cell membrane permeability to water, defined by an Arrhenius relationship (Levin *et al* 1976) as (Eqn.1.9),

$$L_p = L_{pg} \exp \left[ -\frac{E_{Lp}}{R} \left( \frac{1}{T} - \frac{1}{T_R} \right) \right]$$

where  $L_{pg}$  is the permeability of the membrane to water at a reference temperature ( $T_R = 273.15$  K) and  $E_{Lp}$  is the apparent activation energy for the permeability process. A detailed description and the various assumptions made in the development of the water transport model are discussed in main introduction of the thesis.

### 2.2.2 Optimal Cooling Rate

As stated earlier in the introduction, cooling rates that are either “too high” or “too low” can reduce the post thaw survival of the cells either by “intracellular ice formation” or by “solute damage” respectively (Mazur 1972). Based upon this two factor hypothesis of freezing injury, a cooling rate for maximum cell cryosurvival should and does exist between the "high" and "low" rates (McGrath 1988). This has been confirmed experimentally for a variety of cells and the

curve of cell survival plotted as a function of the cooling rate, has a characteristic U-shape as shown in Fig 1.5 (Mazur 1972, Mazur 1984).

Whether a given cooling rate is "too high" or "too low" for a given cell type depends on the various cell parameters including  $L_{pg}$ ,  $E_{Lp}$ ,  $V_b$ ,  $V_o$ , and the available cell membrane surface area (SA). The last three parameters ( $V_b$ ,  $V_o$ , SA) can be collapsed into a single parameter, SA/WV (by defining WV as the initial intracellular water volume or  $WV = V_o - V_b$ ). As different cells have different biophysical parameters, the optimal cooling rate depends on the cell type and there is a wide range of optimal cooling rate values ranging from  $\sim 1$  °C/min (bone marrow cells) to  $\sim 10^3$  °C/min (red blood cells) (Mazur 1970, Mazur 1972). Following Mazur (Mazur 1990) and others (Devireddy *et al* 1998, Devireddy *et al* 2000, Devireddy *et al* 2002), we defined the optimal cooling rate ( $B_{opt}$ ) as the "highest" cooling rate which traps 5% of the initial intracellular water (WV) at an end temperature of  $-15$  °C

### 2.2.3 Numerical Simulations

The water transport equation shown above (Eqns. 1.8 and 1.9) was numerically solved by using a fourth-order Runge-Kutta method to calculate the optimal cooling rate values over a wide range of various cell level parameters. A numerical FORTRAN code was developed and simulations were performed on DELL workstations in the WINDOWS environment, as described in other studies (Devireddy *et al* 1998). The key parameters chosen for this parametric investigation are, permeability of the membrane to water ( $L_{pg}$ ), apparent activation energy ( $E_{Lp}$ ), inactive cell volume ( $V_b$ ), diameter (D), end temperature ( $T_{end}$ ), and the ratio of the available surface area for water transport to the initial volume of intracellular water (SA/WV). For all results presented below  $B_{opt}$  is defined as the cooling rate which traps 5% of WV at  $-15$  °C.

## 2.3 Results and Discussion

Fig 2.1 shows the general variation of the predicted optimal cooling rate ( $B_{opt}$ , °C/min) as a function of reference membrane permeability ( $L_{pg}$ ,  $\mu\text{m}/\text{min-atm}$ ). There is an exact and linear relationship between the inserted change in the value of  $L_{pg}$  and corresponding change in the predicted value of  $B_{opt}$ . This linear relationship is found to extend to any value of  $L_{pg}$  as long as all other parameters are maintained constant. The data is shown in Table 2.2. An examination of the water transport model (Eqns. 1.8 and 1.9), shows that as the permeability ( $L_{pg}$ ) of the membrane increases, the water transport to the extracellular space will also increase and more water will leave the cell in a given time. In other words, the greater the membrane permeability, the larger the net flux across the membrane for any given concentration difference between the intracellular and extracellular spaces. At high permeability values, therefore, the cooling rate

Table 2.2 Linear variation of  $B_{opt}$  with  $L_{pg}$ . The data is taken at  $V_b = 0.4$ , and diameter ( $D$ ) =  $10\mu\text{m}$ .

$E_{Lp} = 10.0 \text{ Kcal/mole}$		$E_{Lp} = 20.0 \text{ Kcal/mole}$	
$L_{pg}$ ( $\mu\text{m}/\text{min-atm}$ )	$B_{opt}$ ( $^{\circ}\text{C}/\text{min}$ )	$L_{pg}$ ( $\mu\text{m}/\text{min-atm}$ )	$B_{opt}$ ( $^{\circ}\text{C}/\text{min}$ )
0.01	5.998	0.01	3.188
0.1	59.98	0.1	31.88
1.0	599.8	1.0	318.8

should be fast enough in order to avoid this severe cell dehydration. On the other hand at low permeability values, the cooling rate should be slow enough to give sufficient time for the cell water to leave the cell and avoid the intracellular ice formation. Thus, the reference membrane

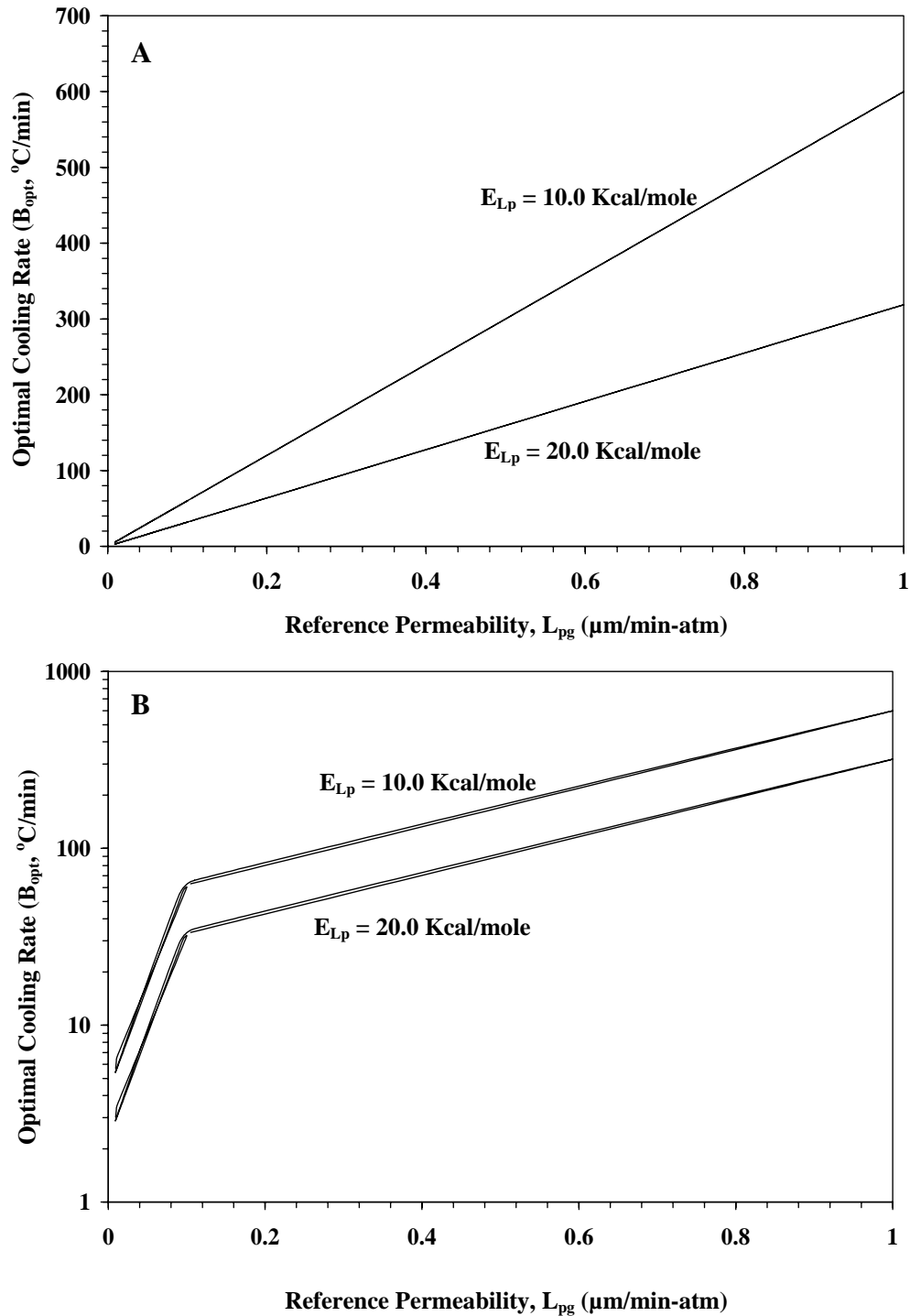


Figure 2.1: The general variation of the predicted optimal cooling rate ( $B_{opt}$ , °C/min) as a function of reference membrane permeability ( $L_{pg}$ ,  $\mu\text{m}/\text{min-atm}$ ).  $B_{opt}$  values are plotted by assuming  $V_b = 0.4$ , diameter ( $D$ ) =  $10.0\mu\text{m}$  and at two different values of  $E_{Lp}$  (10.0 & 20.0 Kcal/mole). The X-axis in Fig 2.1A is in logarithmic scale while Fig 2.1B shows the same data in a linear scale. The  $L_{pg}$  values are shown along the X-axis and the  $B_{opt}$  values are shown along the Y-axis.

permeability has a linear relationship with the predicted optimal cooling rate, as shown in Fig 2.1.

Fig 2.2 and Table 2.3 show the non-linear relationship between the predicted optimal cooling rate ( $B_{opt}$ , °C /min) and the activation energy ( $E_{LP}$ , Kcal/mole). As shown in Fig 2.2, an increase in the value of  $E_{LP}$  causes a decrease in the predicted value of  $B_{opt}$  (see Fig 2.2A; 20% positive change in the value of  $E_{LP}$ ) and vice-versa (see Fig 2.2B; 20% negative change in the value of  $E_{LP}$ ). Also a comparison of Figs 2.2A and 2.2B shows that the change in the  $B_{opt}$  value is higher for a given negative change in  $E_{LP}$  when compared to the change in  $B_{opt}$  value for the same value of positive change in  $B_{opt}$  (see Table 2.3). And finally this non-linear relationship between  $E_{LP}$  and  $B_{opt}$  is seen to be a function of the value of  $E_{LP}$  and for values greater than 50 Kcal/mole, the variation in the predicted optimal cooling rate is almost negligible (see Fig 2.2).

Table 2.3: Non-linear variation of  $B_{opt}$  with  $E_{LP}$ . The data is taken at  $V_b=0.4$ ,  $L_{pg}=1.0\mu\text{m}/\text{min-atm}$  and diameter of  $10\mu\text{m}$ .

$E_{LP}$ (Kcal/mole)	$B_{opt}$ (°C/min)	%Change in $E_{LP}$	% Change in $B_{opt}$
8	686	-20	14.3
10	599.8	0	0
12	525.8	20	-12.3

An examination of Eqn. 1.9 shows that the activation energy ( $E_{LP}$ ) represents the rate at which the permeability of the cell membrane drops with temperature during a freezing process. As the value of activation energy ( $E_{LP}$ ) increases the permeability of the membrane ( $L_p$ ) drops considerably (McGrath 1988, Levin *et al* 1976) and consequently the cooling rate should be slow enough to account for the drop in permeability and is shown in Fig 2.2.

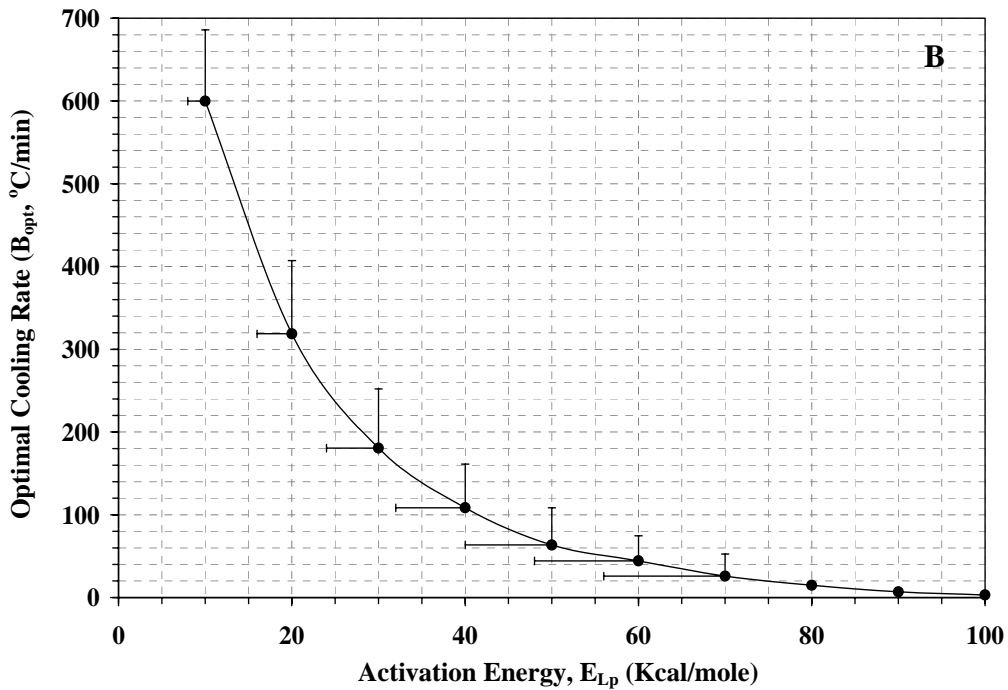
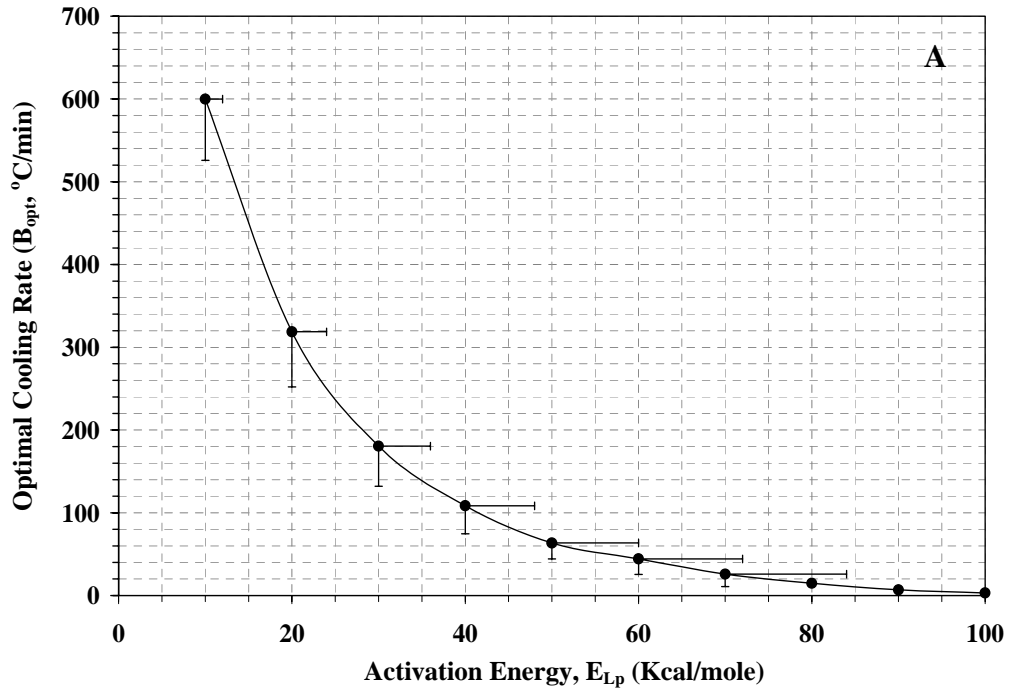


Figure 2.2: Plot of the predicted optimal cooling rate ( $B_{opt}$ , °C /min) as a function of activation energy ( $E_{LP}$ , Kcal/mole) assuming  $L_{pg} = 1.0\mu\text{m}/\text{min-atm}$ ,  $V_b=0.4$ , and diameter ( $D$ ) =  $10\mu\text{m}$ . The error bars represent the non-linear variation of  $B_{opt}$  with  $E_{LP}$ . In Fig 2.2A the error bars represent variation for a positive 20% change in  $E_{LP}$  where as in Fig 2.2B the error bars represent negative 20% change in  $E_{LP}$ . The  $E_{LP}$  values are shown along the X-axis and  $B_{opt}$  values are shown along the Y-axis

In a further parametric investigation the effect of diameter (D) of the cell and inactive cell volume ( $V_b$ ) on the optimal cooling rate ( $B_{opt}$ ) were also studied. These two parameters have a non-linear effect on ' $B_{opt}$ ' value (see Table 2.4). It is observed that as the value of 'D' increases ' $B_{opt}$ ' value decreases and vice versa. In case of ' $V_b$ ' it is reverse. The increase in ' $V_b$ ' value causes the ' $B_{opt}$ ' value to increase and decrease in ' $V_b$ ' value results in decrease of ' $B_{opt}$ ' value. Fig 2.3A & 2.3B shows, respectively, the effect of diameter (D) and  $V_b$  on optimal cooling rate ( $B_{opt}$ ). An increase in diameter of the cell causes an increase in initial intracellular water volume and at the same time the surface area (SA) available for water efflux and inactive cell volume ( $V_b$ ) also increases. But the increase in intracellular water volume for a given increase in

Table 2.4: Variation of  $B_{opt}$  with D and  $V_b$ . Data is taken at  $L_{pg} = 1.0 \mu\text{m}/\text{min-atm}$

<b><math>E_{Lp} = 10.0 \text{ Kcal/mole}</math></b>				<b><math>E_{Lp} = 20.0 \text{ Kcal/mole}</math></b>			
<b>D (<math>\mu\text{m}</math>)</b>	<b><math>B_{opt}</math> (<math>^{\circ}\text{C}/\text{min}</math>)</b>	<b><math>V_b</math></b>	<b><math>B_{opt}</math> (<math>^{\circ}\text{C}/\text{min}</math>)</b>	<b>D (<math>\mu\text{m}</math>)</b>	<b><math>B_{opt}</math> (<math>^{\circ}\text{C}/\text{min}</math>)</b>	<b><math>V_b</math></b>	<b><math>B_{opt}</math> (<math>^{\circ}\text{C}/\text{min}</math>)</b>
5	2305.00	0.2	576.24	5	588.64	0.2	147.16
50	230.5	0.4	768.32	50	58.90	0.4	196.21
100	115.25	0.8	2304.97	100	29.43	0.8	588.64

diameter is more when compared to the increase in surface area which is necessary to remove this excess water. Therefore, the increase in diameter causes an increase in cell water volume and the cooling rate must be slow enough to avoid any possible intracellular ice formation before the optimal percentage of water is trapped inside the cell. Interestingly, at lower values of 'D' a small change in diameter of the cell produces a significant change in optimal cooling rate value.

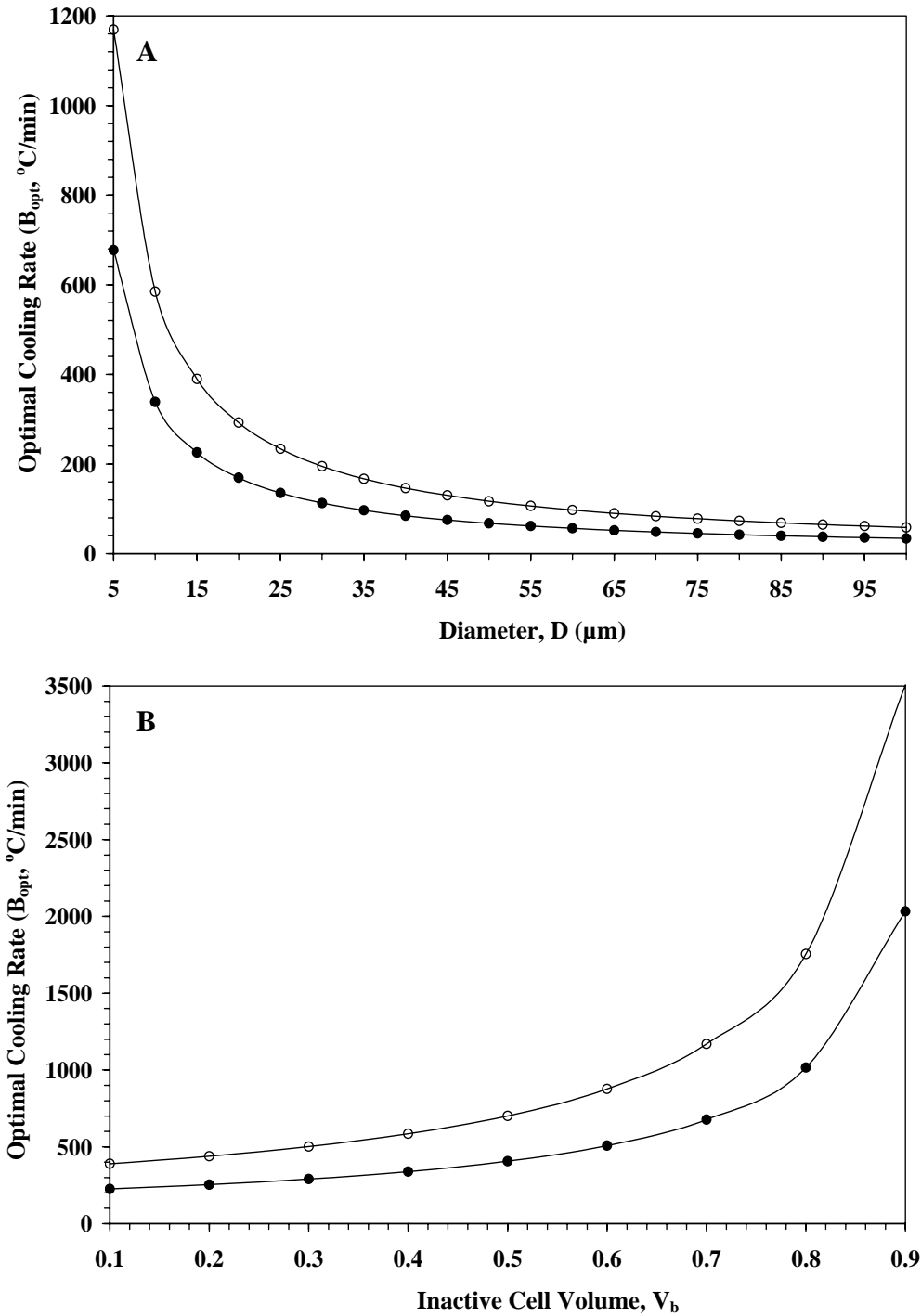


Figure 2.3: Variation of optimal cooling rate ( $B_{opt}$ , °C/min) as a function of diameter,  $D$  (figure A) and inactive cell volume,  $V_b$  (figure B) at different criteria based on activation energy ( $E_{Lp}$ ) of the cell. For Fig 2.3A, the data is taken assuming  $L_{pg} = 1.0 \mu\text{m}/\text{min-atm}$  and  $V_b = 0.4$  where as for Fig 2.3B the data is taken assuming  $L_{pg} = 1.0 \mu\text{m}/\text{min-atm}$  and diameter ( $D$ ) =  $10 \mu\text{m}$ . For both the figures the open circles (-o-) represent  $B_{opt}$  variation at  $E_{Lp} = 10.0 \text{ Kcal/mole}$  and filled circles (-●-) represent  $B_{opt}$  variation at  $E_{Lp} = 20 \text{ Kcal/mole}$ .

This variation reduces gradually as the diameter of the cell increases (see Fig 2.3A). The increase in inactive cell volume ( $V_b$ ) causes the cell water volume to reduce and hence the cooling rate should be fast enough to avoid complete cell dehydration at slower cooling velocities. Therefore, the increase in  $V_b$  should increase the optimal cooling rate ( $B_{opt}$ ) which is also shown in our results. In case of ' $V_b$ ', the variation is small at lower values of ' $V_b$ ', and more at higher values of ' $V_b$ ' (see Fig 2.3B).

For all results shown above, the end temperature at which the optimal percentage of water trapped inside the cell is assumed as  $-15\text{ }^\circ\text{C}$ . In further investigation, we were also interested in knowing the variations in predicted  $B_{opt}$  value when assumed end temperature value is changed. Simulations were performed in a range of end temperatures ( $-15\text{ }^\circ\text{C}$  to  $-45\text{ }^\circ\text{C}$ ) in steps of  $-15\text{ }^\circ\text{C}$ . Fig 2.4 shows the non-linear relationship between the predicted optimal cooling rate ( $B_{opt},\text{ }^\circ\text{C}/\text{min}$ ) and the assumed end temperature ( $T_{end},\text{ }^\circ\text{C}$ ). As shown in Fig 2.4, an increase in the value of  $T_{end}$  causes a decrease in the predicted value of  $B_{opt}$  (see Fig 2.4A) and vice versa. As  $T_{end}$  increases, the time available for the cell to reach the assumed end temperature value (at which water transport shuts off and optimal % of water is trapped inside the cell) will be less. Therefore, the cooling rate must be slow in order to allow sufficient time for water to leave the cell and join the extracellular space before the cell reaches assumed optimal end temperature value. The increase in  $T_{end}$  value should decrease the  $B_{opt}$  value which is also shown in our results (Fig 2.4A). Fig 2.4B shows the  $B_{opt}$  variation with  $T_{end}$  at  $E_{Lp} = 100.0\text{Kcal/mole}$ . As it is explained earlier, the variation in  $B_{opt}$  value is almost negligible at higher values of  $E_{Lp}$  and hence the  $B_{opt}$  values represent almost straight lines as shown in Fig 2.4B.

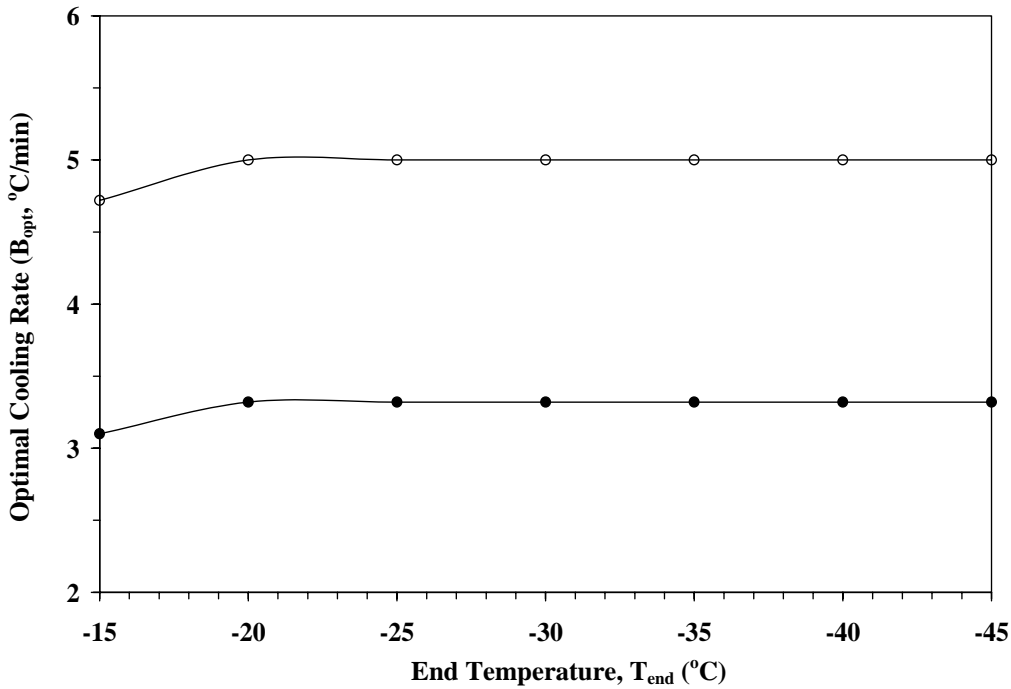
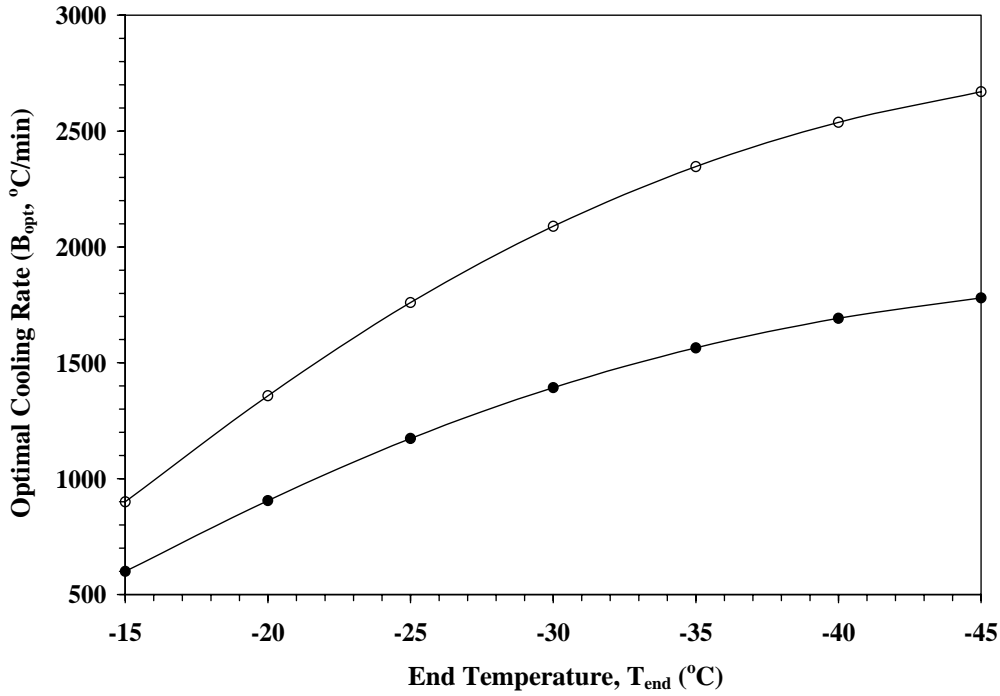


Figure 2.4: The general variation of the predicted optimal cooling rate ( $B_{opt}$ , °C/min) as a function of end temperature ( $T_{end}$ , °C).  $B_{opt}$  values are plotted by assuming  $L_{pg} = 1.0\mu\text{m}/\text{min-atm}$  and diameter ( $D$ ) =  $10\mu\text{m}$ . For both the figures the open circles (-o-) represent  $B_{opt}$  variation at  $V_b = 0.6$  and filled circles (-●-) represent  $B_{opt}$  variation at  $V_b = 0.4$ . Fig 2.4A represents  $B_{opt}$  variation at  $E_{Lp} = 20\text{Kcal}/\text{mole}$  whereas Fig 2.4B at  $E_{Lp} = 100.0\text{Kcal}/\text{mole}$ . The  $T_{end}$  values are shown along the X-axis and the  $B_{opt}$  values are shown along the Y-axis.

In a further investigation, the above results are critically analyzed and by observing the effect of  $V_b$  and diameter (D) on optimal cooling rate (both are having an opposite effect on  $B_{opt}$ ), we were interested to find out the cumulative effect of these two parameters on the optimal cooling rate. The diameter (D) of the cell (or in the case of a tissue cell unit, the Krogh Model

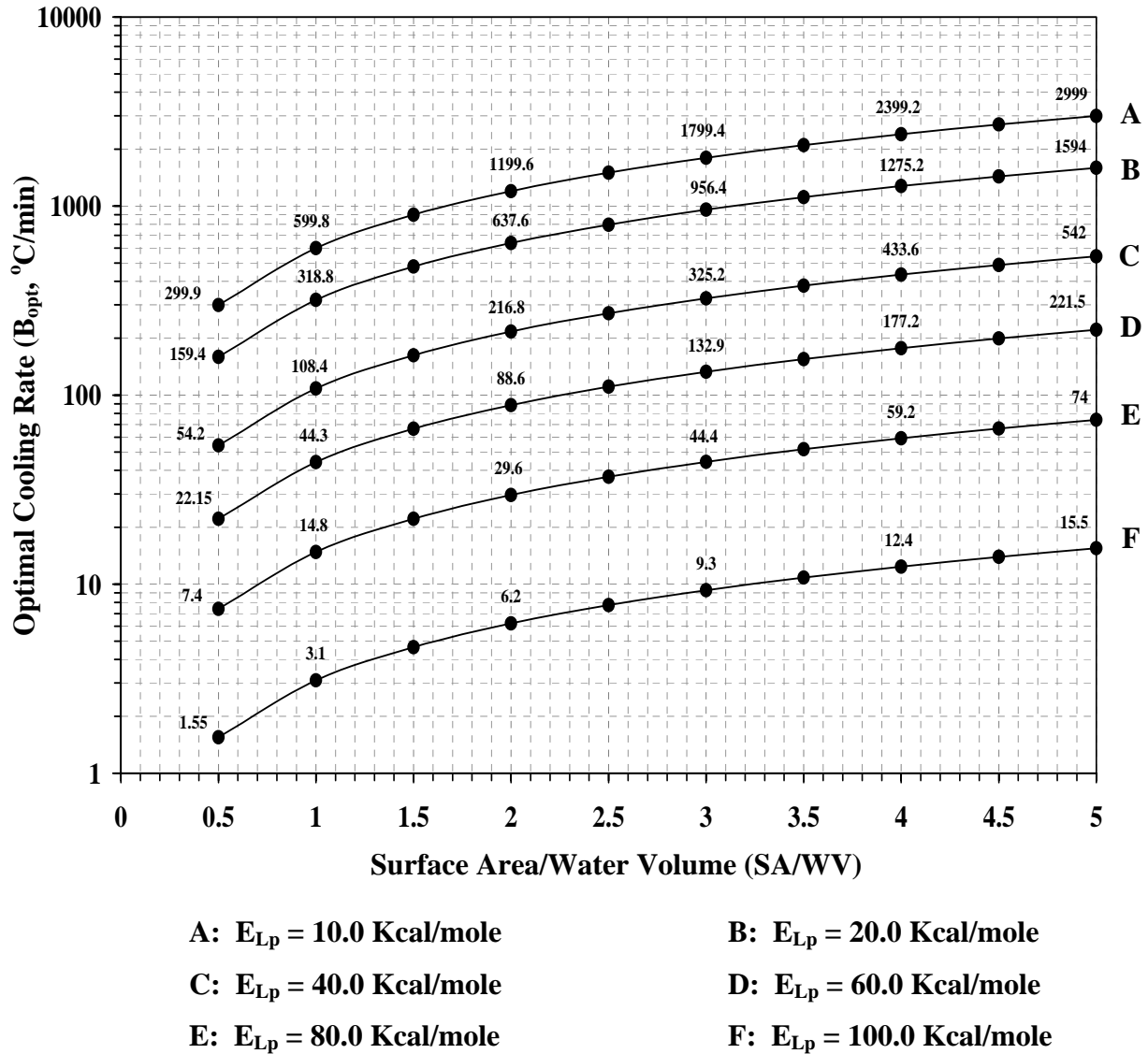


Figure 2.5: Plot of the predicted optimal cooling rate ( $B_{opt}$ , °C /min) as a function of water volume/surface area (SA/WV) at  $L_{pg} = 1.0 \mu\text{m}/\text{min-atm}$  and different  $E_{Lp}$  values. The SA/WV values are shown along the X-axis and  $B_{opt}$  values are shown along the Y-axis in logarithmic scale.

dimensions,  $\Delta X$ ,  $r_v$  and  $L$ ), the initial isotonic cell volume ( $V_o$ ), and the inactive cell volume ( $V_b$ ) were collapsed into a single parameter SA/WV. Note that for a spherical cell the available membrane surface area (SA) is modeled as  $4\pi r^2$  and the isotonic cell volume ( $V_o$ ) as  $\frac{4}{3}\pi r^3$  while for a tissue cell unit the SA is modeled as  $2\pi r_v L$  and  $V_o$  as  $\Delta X^2 - \pi r_v^2 L$  (Devireddy *et al* 2000; Devireddy and Bischof 2003).

Fig 2.5 shows the general variation of the predicted optimal cooling rate ( $B_{opt}$ , °C /min) as a function of SA/WV ratio at different  $E_{Lp}$  values. As shown, for a given value of  $E_{Lp}$ , the numerically predicted  $B_{opt}$  values have an exact and linear variation with the SA/WV ratio (similar to the relationship between  $L_{pg}$  and  $B_{opt}$ , shown in Fig 2.1). For example the  $B_{opt}$  value at SA/WV = 0.5 and  $E_{Lp} = 20.0$  Kcal/mole is 159.4 °C/min and when the value of SA/WV increases by a factor 10 the  $B_{opt}$  value increases by the same factor of 10 (i.e., at SA/WV = 5.0, the  $B_{opt}$  is 1594.0 °C/min). This linear variation is found to extend to any ratio of surface area to water volume (SA/WV) as long as all other investigated parameters remain constant.

Mechanistically this relationship can be explained as follows: For a given intracellular water volume (WV), an increase in the surface area of the membrane (SA) (or an increase in the SA/WV ratio) allows larger amount of intracellular water to leave the cell and severe dehydration would become the principal mechanism for cell damage. To circumvent this, the cooling rate needs to be fast enough to trap the optimal percentage of cell water and convert into ice before the cell gets completely dehydrated. Conversely, decrease in the value of SA (or decrease in SA/WV ratio) lowers the rate of water leaving the cell and consequently the cooling rate should decrease and provide sufficient time for the cell water to leave the cell. Therefore the increase in the ratio of the SA/WV should increase the optimal cooling rate and vice versa, as shown in Fig 2.5.

The observed relationship between SA/WV and  $B_{opt}$  can be used to collapse all of the curves shown in Fig 2.5 into a single curve by taking  $E_{Lp}$  values on X-axis and plotting the cooling rate values at SA/WV = 1.0 as shown in Fig 2.6. We call Fig 2.6 as the Generic Optimal Cooling Rate Chart (GOCRC). GOCRC shows the variation of cooling rate ( $B_{GOCRC}$ , °C/min) values as a function of activation energy ( $E_{Lp}$ , Kcal/mole). The  $B_{GOCRC}$  values are plotted for different  $E_{Lp}$  values at  $L_{pg} = 1.0 \mu\text{m}/\text{min-atm}$  and SA/WV = 1.0 (these values are chosen since it

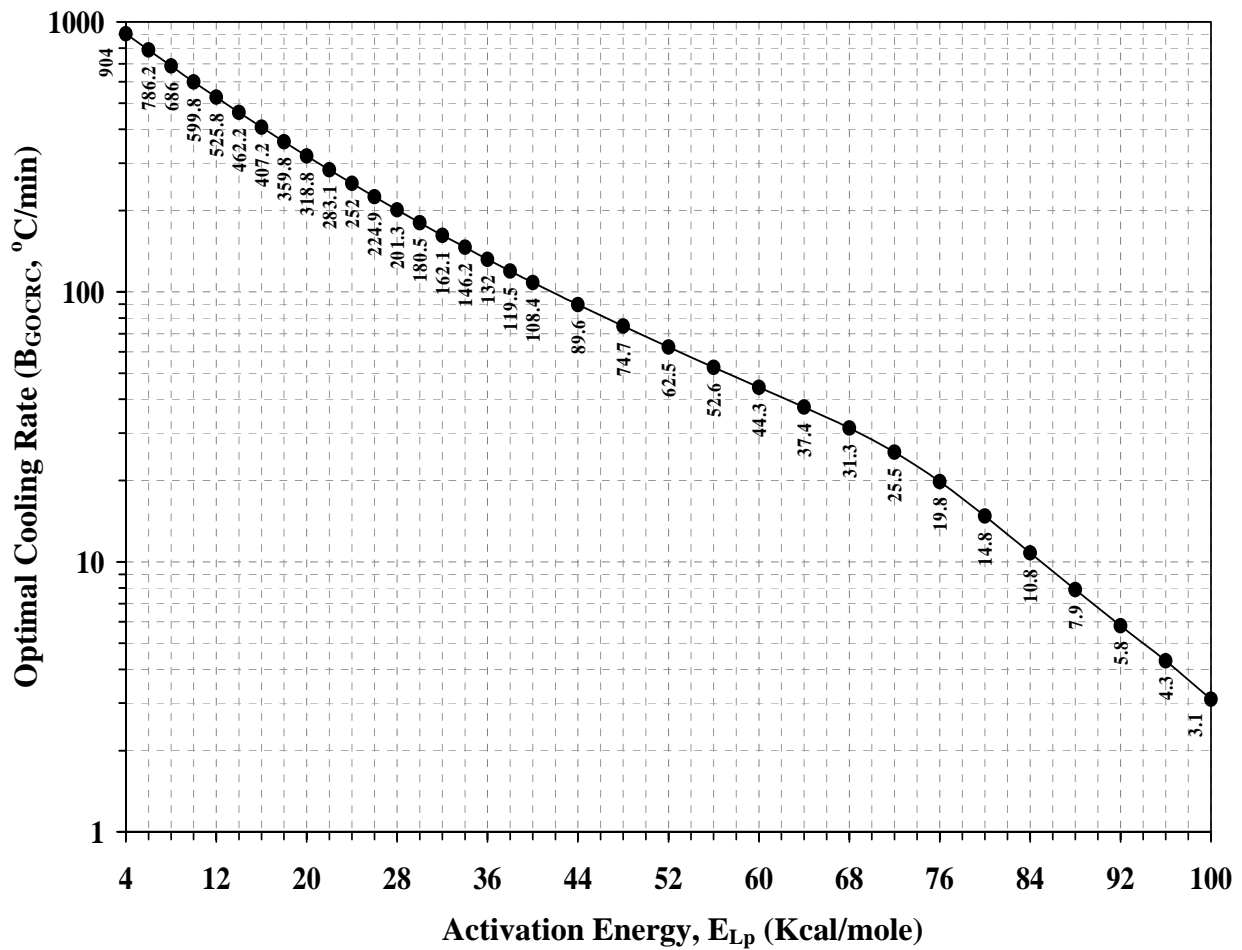


Figure 2.6: “Generic Optimal Cooling Rate Chart (GOCRC)”. Predicted GOCRC cooling rates are plotted as a function of activation energy ( $E_{Lp}$ , Kcal/mole) at  $L_{pg} = 1.0 \mu\text{m}/\text{min-atm}$  and WV/SA = 1.0. The  $E_{Lp}$  values are shown along X-axis and  $B_{GOCRC}$  values are shown along Y-axis in logarithmic scale.

is trivial to calculate  $B_{opt}$  at other values of  $L_{pg}$  and  $SA/WV$ ). As there is an exact linear relationship between  $L_{pg}$ ,  $SA/WV$  and  $B_{opt}$  values (as shown in Figs 2.1 and 2.5), a simple algebraic equation now relates the cooling rate values on Y- axis ( $B_{GOCRC}$ ) with optimal cooling rate value for any given arbitrary biological system as,

$$B_{opt} = B_{GOCRC} * (L_{pg})_a * \left( \frac{SA}{WV} \right)_a \quad (2.1)$$

where ' $(L_{pg})_a$ ' and ' $(SA/WV)_a$ ' are the actual cell level parameters of the biological system for which the predicted optimal cooling rate ( $B_{opt}$ ) is to be calculated. The ' $B_{GOCRC}$ ' in the RHS of the equation is the cooling rate shown on the Y-axis of the GOCRC corresponding to the given value of  $E_{Lp}$  or  $(E_{Lp})_a$ .

As stated earlier, to generate the Generic Optimal Cooling Chart (GOCRC) shown in Fig 2.6, we assigned values to two model parameters:  $T_{end}$  (-15 °C) and  $\%W_T$  (5%). However, similar GOCRC s for other values of  $T_{end}$  and  $\%W_T$  have been generated for appropriate use (data not shown). We then compared our numerical results from GOCRC with several experimental optimal cooling rate values for various cell types, obtained from an extensive investigation of published literature (see Table 2.5 and Fig 2.7). As shown in Fig 2.7 and Table 2.5, there is reasonably good agreement between the  $B_{opt}$  values obtained using GOCRC and empirically determined experimental values (with the exception of AT-1 cells, a tumor cell line). Although most of the experimental optimal cooling rate values for various cells are in the presence of cryoprotective agents (CPAs) and our numerical model of water transport doesn't include the addition of CPAs during a freezing process (Karlsson *et al*), we still find a reasonably good agreement between the experimentally predicted  $B_{opt}$  values and the corresponding values using GOCRC (shown in Table 2.5). This is possibly because  $(L_{pg})_a$  and  $(E_{Lp})_a$  values used in

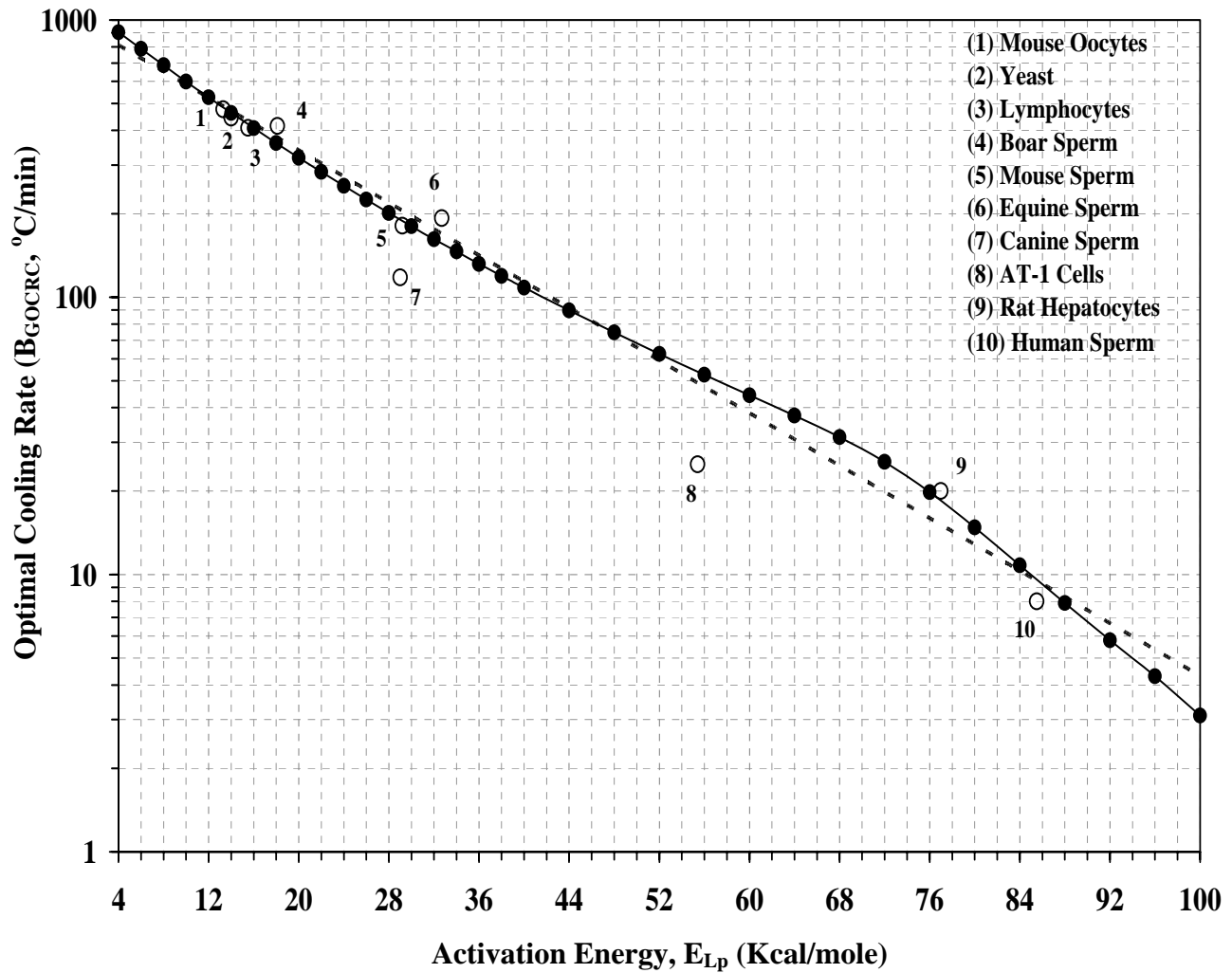


Figure 2.7: “Generic Optimal Cooling Rate Chart (GOCRC)”. A comparison of the GOCRC predicted optimal cooling rate values and experimentally determined values for a variety of biological systems (open circles). The dotted line represents a curve fitting used to generate a mathematical equation for  $B_{GOCRC}$  value,  $B_{GOCRC} = 1009.5 * \exp^{(-0.0546 * E_{LP})}$  (with a goodness of fit of  $R^2 = 0.994$ ). The  $E_{LP}$  values are shown along X-axis and  $B_{GOCRC}$  values are shown along Y-axis in logarithmic scale.

Eqn. (2.1) to determine the  $B_{opt}$  from GOCRC are in fact obtained by curve-fitting experimental water transport data to a model of water transport that does include the effect of CPAs during a freezing process.

Table 2.5: Experimental vs. GOCRC Optimal Rates of Cooling

Cell System	$L_{pg}$ ( $\mu\text{m}/\text{min-atm}$ )	$E_{Lp}$ (Kcal/mole)	SA/WV	$B_{opt}$ (Expt) ( $^{\circ}\text{C}/\text{min}$ )	$B_{opt}$ (GOCRC) ( $^{\circ}\text{C}/\text{min}$ )	% Error with GOCRC	References
Yeast	0.072	14.0	1.39	44.5	46.2	-3.8	Levin <i>et al</i> 1979 McGrath 1985
Lymphocytes	0.1	15.5	0.735	30	31.6	-5.3	Scheiwe1984 Devireddy <i>et al</i> 1998
Mouse Oocytes	0.044	13.3	0.0954	2.0	2.1	-5.0	Leibo 1980 Levin <i>et al</i> 1979
Rat Hepatocytes	0.009	77	0.5515	0.1	0.09	10.0	Harris <i>et al</i> 1991 Toner <i>et al</i> 1992 Smith <i>et al</i> 1998
Mouse Spermatozoa	0.01	29.2	11.1	20.1	21.1	5.0	Devireddy <i>et al</i> 1999
Human Spermatozoa	0.04	33.2	6.2	2.0	2.2	-10.0	Henry <i>et al</i> 1993 Devireddy <i>et al</i> 2000
Equine Spermatozoa	0.02	32.7	7.5	28.9	22.2	23.2	Devireddy <i>et al</i> 2002
Boar Spermatozoa	0.005	18.1	16.35	33.9	29.8	12.0	Devireddy <i>et al</i> 2003
Canine Spermatozoa	0.005	29	15.6	9.2	14.4	-56.0	Thirumala <i>et al</i> 2003
AT-1 Tumor Cells	2.71	55.4	0.3	10.5	43.9	-318.0	Smith <i>et al</i> 1997

And finally, the use of GOCRC was further simplified by developing a simple mathematical equation by curve fitting to the values in GOCRC (the dotted line in Fig 2.7) and is given by,

$$B_{GOCRC} = 1009.5 * \exp^{(-0.0546 * E_{Lp})} \quad (2.2)$$

By substituting Eqn. (2.1) in Eqn. (2.2), we developed a simple mathematical equation to determine the value of  $B_{opt}$  for a biological cell or tissue section, once  $(L_{pg})_a$ ,  $(E_{Lp})_a$  and  $(SA/WV)_a$  are known *a priori*. We refer to this equation as the Generic Optimal Cooling Rate Equation (GOCRE) and is given as, (2.3)

$$B_{opt} = 1009.5 * \exp^{(-0.0546 * E_{Lp,a})} * (L_{pg})_a * \left( \frac{SA}{WV} \right)_a \quad (2.3)$$

Clearly, the use of Eqn. (2.3) or Fig 2.6 represents a greatly simplified procedure to predict the optimal rate of freezing for an arbitrary biological system.

## 2.5 Conclusion

The effect of various cell level parameters on the predicted optimal cooling rate of an arbitrary biological system has been thoroughly investigated using a well-defined water transport model. The key parameters investigated were, reference permeability of the membrane to water ( $L_{pg}$ ), apparent activation energy ( $E_{Lp}$ ), and the ratio of the available surface area for water transport to the initial volume of intracellular water ( $SA/WV$ ). By analyzing the relationships between  $L_{pg}$ ,  $E_{Lp}$ ,  $SA/WV$  and  $B_{opt}$ , a Generic Optimal Cooling Rate Chart (GOCRC) and a Generic Optimal Cooling Rate Equation (GOCRE) were developed. The use of GOCRC and

GOCRC greatly simplify the process of predicting the optimal cooling rate values for an arbitrary biological system whose values of  $L_{pg}$ ,  $E_{Lp}$  and  $SA/WV$  are known *a priori*.

## Chapter 3

### **Cryopreservation of Canine Spermatozoa: Theoretical Prediction of Optimal Cooling Rates in the Presence and Absence of Cryoprotective Agents**

#### **3.1 Introduction**

The past few years have seen significant advances in the genome mapping of several canine species (Ostrander *et al* 2000, Ostrander and Kruglyak 2000). More importantly, these studies have found that several canine genetic diseases are true homologs of those in humans (Ostrander *et al* 2000), i.e., making the dog an important model for the study of various human genetic disorders. Further acceptance and widespread use of dogs as animal models requires improved cryopreservation protocols of canine sperm cells. To this end several studies have reported the successful cryopreservation of canine sperm cells and in some cases even the birth of live pups using frozen/thawed sperm cells (Foote 1964, Linde-Forsberg and Forsberg 1989, England 1993, Silva *et al* 1996). However, the effective and widespread use of frozen canine sperm is still limited, mainly because of its association with low fertility and indifferent results (Dobrinski *et al* 1993, Fontbonne and Badinand 1993, Linde-Forsberg *et al* 1999, Pinto *et al* 1999). Clearly, further usage of frozen/thawed canine sperm requires a firm biophysical understanding of the cryopreservation process. The bulk of our understanding in the cryopreservation of canine sperm (and mammalian sperm in general) is still empirical in nature, since the unique size and morphology of mammalian sperm limit the applicability of standard cellular cryomicroscopy techniques to measure the biophysical response (water transport and intracellular ice formation) in sperm cells during freezing. However, a recent advance in measurement methodology, namely a differential scanning calorimetry (DSC) based technique

(Devireddy and Bischof 2003), has improved our knowledge of the water transport response during freezing in several mammalian gametes, including mouse (Devireddy *et al* 1999), human (Devireddy *et al* 2000), and horse (Devireddy *et al* 2002). The DSC technique will also be used in the present study to improve our understanding of the biophysical response during freezing of canine sperm cells suspensions.

As discussed in the main introduction, during freezing of any cell suspension, ice nucleates initially in the extracellular space causing an osmotic gradient to be set up across the intracellular isotonic solution and the freeze-concentrated extracellular solution (Mazur 1963, Mazur 1984). Depending on whether the cooling rate is “slow” or “fast”, the intracellular water permeates across the cell membrane and joins the extracellular ice phase or freezes and forms ice inside of the cell, respectively. In most cases, cells undergoing ice formation inside the cells or intracellular ice formation (IIF) are rendered osmotically inactive (lysed), due to the loss of cell membrane integrity (Mazur 1970, Meryman 1996). Similarly cells which experience a severe loss of intracellular water are also rendered osmotically inactive (Lovelock 1953). Both IIF and long exposures to high solute concentrations are lethal to cells. So cooling rates, which are either “too slow” or “too fast”, can and do kill cells, therefore an “optimal” cooling rate should, and does, exist between the “slow” and “fast”. This has been confirmed experimentally for a variety of cells, and the curve of cell survival plotted as a function of the cooling rate has a characteristic inverted U-shape (Fig 1.5) (Mazur 1972). Whether a prescribed cooling rate is too “slow” or too “fast”, is a function of cell membrane permeability to water and the probability that any water remaining trapped within the cell at any given subzero temperature will nucleate and turn to ice. Differences in membrane permeability to water and the probability of IIF result in different

“optimal” cooling rates for different cells. Therefore, to optimize a cryopreservation protocol it is important to measure the cell membrane’s permeability to water.

A paucity of knowledge regarding the water permeability parameters during freezing in the presence of extracellular ice and cryoprotective agents (CPAs) is the limiting factor in reconciling the dichotomy between the numerically predicted and experimentally determined optimal rates of freezing in canine (and in general mammalian) gametes. Traditional light microscopy based techniques cannot be used to obtain the relevant biophysical parameters during freezing in sperm cells because of their highly non-spherical shape and small dimensions. In the present study a well established shape independent Differential Scanning Calorimeter (DSC) technique was used to measure the dehydration response during freezing of ejaculated canine sperm cells. The DSC is an instrument, which measures heat releases during phase change processes as a function of time and temperature. In the DSC technique, two heat releases from the same cell suspension (or tissue system) are measured: i) during freezing of osmotically active (live) cells in media (where the intracellular water is being transported across the membrane to freeze in the extracellular space) and; ii) during freezing of osmotically inactive (dead) cells in media. The difference in heat release measured between the two cooling runs is correlated to water transport. This has been demonstrated in a variety of cellular systems including murine (Devireddy *et al* 1999), human (Devireddy *et al* 2000), and equine (Devireddy *et al* 2002) sperm cell suspensions (see a recent review by Devireddy and Bischof 2003, for other cell types).

In this study volumetric shrinkage during freezing of canine sperm cell suspensions was obtained at cooling rates of 5 and 10 °C/min in the presence of extracellular ice and CPAs (6 different combinations of freezing media were used, ranging from a media with no CPAs, and those with 0.5%, 3% and 6% glycerol and with 0.5% and 3% Me<sub>2</sub>SO). Using previously

published data, the canine sperm cell was modeled as a cylinder of length 105.7  $\mu\text{m}$  and a radius of 0.32  $\mu\text{m}$  with an osmotically inactive cell volume,  $V_b$ , of  $0.6V_o$ , where  $V_o$  is the isotonic cell volume. By fitting a model of water transport to the experimentally obtained volumetric shrinkage data the best fit membrane permeability parameters ( $L_{pg}$  and  $E_{Lp}$ ) were determined. These parameters are significantly different than previously published parameters for canine and other mammalian sperm obtained at suprazero temperatures and at subzero temperatures in the absence of extracellular ice. The parameters obtained in this study also suggest that optimal rates of freezing canine sperm cells ranges from 10 to 30  $^{\circ}\text{C}/\text{min}$ ; these theoretical cooling rates are found to be in close conformity with previously published but empirically determined optimal cooling rates. Numerical simulations of water transport in canine sperm cells were then performed under a variety of cooling rates (5 to 100  $^{\circ}\text{C}/\text{min}$ ) using the experimentally determined membrane permeability parameters. The simulation results were analyzed to predict the amount of water left in the cell after dehydration ceased, in the absence of IIF and the “optimal cooling rates” for canine sperm cryopreservation.

## **3.2 Materials and Methods**

### **3.2.1 Collection and Isolation of Sperm Cells**

Eight mature male Beagle dogs were housed in an indoor kennel, fed a dry kibble dog food, and had water provided ad libitum. All animal care and semen collection procedures were performed with approval from the Louisiana State University Institutional Animal and Care Use Committee. Semen was collected once each week from each dog by manual stimulation of the penis with no female present. For the semen collection, the penis was massaged externally through the sheath until a slight erection was obtained. The prepuce was pushed caudally behind the bulbus glandis to expose the slightly erect penis. A plastic artificial vagina end cone (Agtech

Inc., P.O. Box 1222, Manhattan, KS 66502) was placed over the protruded penis and circumferential pressure was applied posterior to the bulbus glandis to stimulate erection and ejaculation. The pre-sperm and sperm rich fractions of semen were collected into the artificial vagina end cone. Each individual semen sample was immediately assessed for progressive motility and then transported to a laboratory for a complete semen analysis. After the analysis, the eight samples were pooled and extended 1:1 v:v with a commercial skim milk semen extender (E-Z Mixin® -"OF", Animal Reproduction Systems, 14395 Ramona Avenue, Chino, CA 91710). The extended sample was then transported to the LSU bioengineering laboratory for DSC experiments. For DSC experiments in the absence of CPA, sperm were concentrated by gentle centrifugation (300x g, room temperature) for 5 min by resuspension in residual supernatant. DSC experiments were also conducted in the presence of 2 permeating CPAs (glycerol, and dimethylsulfoxide or Me<sub>2</sub>SO) at various concentrations (v/v) ranging from 0.5% to 6%. Canine sperm cells were loaded with three different concentrations of glycerol (0.5%, 3% and 6%) and with two different concentrations of Me<sub>2</sub>SO (0.5% and 3%)<sup>1</sup>. Stepwise addition of CPAs was performed to minimize the osmotic injury or the volumetric excursions of the canine sperm cells during the CPA loading process (Gao *et al* 1995, Devireddy *et al* 1999, Devireddy *et al* 2000). After the addition of CPAs, the samples were concentrated by gentle centrifugation (as described earlier) and water transport (DSC) experiments were completed within 3 to 6 hours of sperm isolation.

---

<sup>1</sup> As will be shown in the results, the effect of glycerol and dimethylsulfoxide at a given concentration on the canine sperm permeability parameters is statistically similar, if not exactly the same. Therefore, experiments at the highest concentration (6%) of dimethylsulfoxide were deemed to be superfluous and hence not performed.

### 3.2.2 DSC Experiments

The DSC dynamic cooling experiments were performed on concentrated canine sperm samples in standard aluminum sample pans (Perkin Elmer Corporation, Norwalk, Conn.) in the presence of *P. syringae* (ATCC Rockville, MD), a natural ice nucleator. As described earlier, ~200  $\mu\text{l}$  of extended semen was concentrated by centrifugation (300x g) for 5 minutes, at room temperature and resuspended in ~25  $\mu\text{l}$  of residual supernatant. Approximately 10  $\mu\text{l}$  of this sperm suspension was loaded in a DSC sample pan with ~0.5 mg *Pseudomonas syringae* (ATCC Rockville, MD). The concentration of the sperm suspension used in the DSC experiments ranged from  $200 \times 10^6$  to  $700 \times 10^6$  cells/ml. The DSC dynamic cooling protocol used to measure the water transport out of canine sperm is the same as reported in earlier studies on mammalian sperm cells (Devireddy *et al* 1999, Devireddy *et al* 2000, Devireddy *et al* 2002) and will not be repeated here in the interest of brevity.

### 3.2.3 Translation of Heat Release to Cell Volume Data for Dynamic Cooling

The heat release measurements of interest are  $\Delta q_{dsc}$  and  $\Delta q(T)_{dsc}$  which are the total and fractional difference between the heat releases measured by integration of the heat flows during freezing of osmotically active (live) cells in media and during freezing of osmotically inactive (dead) cells in media. This difference in heat release has been shown to be related to cell volume changes in several biological systems (Devireddy *et al* 1998) as,

$$\frac{V_o - V(T)}{V_o - V_b} = \frac{\Delta q(T)_{dsc}}{\Delta q_{dsc}}. \quad (3.1)$$

We can rearrange this equation to measure water transport data from the DSC measured heat releases  $\Delta q(T)_{dsc}$  and  $\Delta q_{dsc}$  as,

$$V(T) = V_o - \frac{\Delta q(T)_{dsc}}{\Delta q_{dsc}} \cdot (V_o - V_b). \quad (3.2)$$

Note that the DSC measured heat release readings  $\Delta q(T)_{dsc}$  and  $\Delta q_{dsc}$  are obtained separately at 5 °C/min (data not shown) and at 10 °C/min (Fig 1.4 (thermogram at 10 °C/min, without CPAs); for detailed explanation of the thermogram see the main introduction of the thesis)) both in the absence and presence of CPAs. The unknowns needed in Eqn. 3.2 apart from the DSC heat release readings are  $V_o$  (the initial or the isotonic cell volume) and  $V_b$  (the osmotically inactive cell volume) and are taken from published values in the literature (Hansel and McEntee 1970, Kleinhans *et al* 1992, Du *et al* 1994, Goa *et al* 1997).

To ensure the accuracy and repeatability of the experimental data, a set of calibration and control experiments were performed as detailed previously for a DSC-7 (Perkin Elmer Corporation, Norwalk, CT) machine (Devireddy *et al* 1998, Devireddy and Bischof 1998, Devireddy *et al* 1999(c)) and is discussed in detail in the main introduction of the thesis. One of these tests was to check if the measured heat release difference is comparable to the expected value based on the total volume of cell water present in the DSC pan. The total volume of cell water in the DSC sample ( $V$ ) = number of cells • water volume in a single sperm cell =  $\sim 10^9$  (cells) •  $35 \cdot 0.4 \cdot 10^{-18}$  (m<sup>3</sup>/cell) =  $14 \cdot 10^{-9}$  (m<sup>3</sup>). Assuming that the cell water has a density of 1000 kg/m<sup>3</sup>, this translates to 0.014 mg of cell water per mg of total sample. Thus, the expected value of  $\Delta q_{dsc}$  per mg of DSC sample = mass of cell water per mg of total sample • latent heat of fusion of water =  $0.014 \cdot 335 = 4.7$  mJ/mg of total sample (which agrees quite closely with the measured values ranging from 4 to 6 mJ/mg).

A second test was to compare the heat release measured during the final cooling run,  $q_{final}$  with the DSC measured heat release from a separate control experiment composed of only osmotically inactive (or lysed) canine sperm cells and the magnitude of the heat releases were found to be within  $\pm 1\%$ . This suggests that the fast cooling run in the DSC protocol (100 °C/min to -150 °C) compromised the membrane integrity of all the canine sperm cells in the sample. Further support of this observation was obtained when  $\sim 97\%$  of canine sperm cells forced open from the DSC pan after the fast cooling run stained with Propidium Iodide (PI, dead cell stain) and  $\sim 3\%$  stained with SYBR-14 (live cell stain) (Garner *et al* 1994, Garner and Johnson 1995).

### 3.3 Water Transport Model and Numerical Methods

Kedem and Katchalsky (1958) proposed a model for water and solute transport in response to chemical potential gradients based on irreversible thermodynamics. The Kedem and Katchalsky model consisted of two differential equations which describe the water and CPA flux across the membrane (Kedem and Katchalsky 1958). If the flux of CPA is negligible in comparison to the water flux (Gilmore *et al* 1995, McCaa *et al* 1991), then the Kedem-Katchalsky model reduces to a model which assumes only water transport, as proposed by Mazur (1963) and later modified by Levin *et al.* (1976). The water transport model of Mazur was further modified to incorporate the presence of CPAs on the volumetric shrinkage response of cells during freezing as (Karlsson *et al* 1993, Karlsson *et al* 1994),

$$\frac{dV}{dT} = - \frac{L_p A_c R T}{B v_w} \left[ \ln \frac{(V_o - V_b - n_{cpa} v_{cpa}) / v_w}{(V_o - V_b - n_{cpa} v_{cpa}) / v_w + (\varphi_s n_s + n_{cpa})} - \frac{\Delta H_f v_w \rho}{R} \left( \frac{1}{T_R} - \frac{1}{T} \right) \right] \quad (3.3)$$

with  $L_p$ , the sperm cell membrane permeability to water defined by Levin et al. (1976) as,

$$L_p = L_{pg}[cpa] \exp\left(-\frac{E_{Lp}[cpa]}{R}\left(\frac{1}{T} - \frac{1}{T_R}\right)\right) \quad (3.4)$$

where,  $L_{pg}[cpa]$  is the reference membrane permeability at a reference temperature,  $T_R$  (= 273.15 K);  $E_{Lp}[cpa]$  is the apparent activation energy (kJ/mol) or the temperature dependence of the cell membrane permeability;  $V$  is the sperm cell volume at temperature,  $T$  (K);  $A_c$  is the effective membrane surface area for water transport, assumed to be constant during the freezing process;  $V_o$  and  $V_b$  are the isotonic (initial) and osmotically inactive sperm cell volumes, respectively.

In this study, the canine sperm cell is modeled as a long cylinder with length ( $L$ ) 105.7  $\mu\text{m}$  and a radius ( $r_o$ ) of 0.32  $\mu\text{m}$  which translates to  $V_o \sim 34 \mu\text{m}^3$  and  $A_c \sim 212 \mu\text{m}^2$  (Hansel and McEntee 1970, Cummins and Woodall 1985, Rodriguez-Martinez *et al* 1993). The osmotically inactive cell volume,  $V_b$  was assumed to be  $0.6V_o$  a value within the range reported for a variety of mammalian sperm (Du *et al* 1994, Goa *et al* 1997, Kleinhans *et al* 1992);  $R$  is the universal gas constant (8.314 J/mol K);  $B$  is the constant cooling rate (K/min);  $n_{cpa}$  is the number of moles of salt;  $v_{cpa}$  is the molar volume of CPA ( $73.3 \times 10^{12} \mu\text{m}^3/\text{mole}$  for glycerol and  $69.0 \times 10^{12} \mu\text{m}^3/\text{mole}$  for DMSO);  $v_w$  is the molar volume of water ( $18 \times 10^{12} \mu\text{m}^3/\text{mole}$ );  $\phi_s$  is the disassociation constant for salt (= 2);  $n_s$  is the number of moles of salt (=  $C_i \cdot (V_o - V_b)$ , where  $C_i$  is the initial cell osmolality, 0.285M);  $\Delta H_f$  is the latent heat of fusion of water (335 mJ/mg);  $\rho$  is the density of water ( $1000 \text{ kg/m}^3$ ). Note that when  $n_{cpa}$  is zero (i.e. no CPA is present), Eqns. (3.3) and (3.4) reduce to the “water transport” model (Eqns. 1.8 and 1.9) as described by

Mazur (1970) and Levin *et al.* (1976) and  $L_p$  is an Arrhenius function of  $L_{pg}$  and  $E_{Lp}$ . The two unknown membrane permeability parameters of the model either  $L_{pg}$  [cpa] and  $E_{Lp}$  [cpa] in the presence of CPA or  $L_{pg}$  and  $E_{Lp}$  in the absence of CPA, are determined by curve-fitting the water transport model to experimentally obtained volumetric shrinkage data during freezing. The various assumptions made in the development of Mazur's model of water transport are discussed in detail elsewhere (Toner 1993, McGrath 1988, Devireddy *et al* 1999(b)).

### 3.3.1 Numerical Methods

A nonlinear least squares curve fitting technique was implemented using a computer program to calculate the membrane permeability parameters that best fit the volumetric shrinkage data as previously described by Bevington and Robinson (1992). The optimal fit of Eqn. (3.3) to the experimental data was obtained by selecting a set of parameters which minimized the residual variance,  $\chi^2$ , and maximized a goodness of fit parameter,  $R^2$  (Montgomery and Runger 1994). In order to predict the membrane permeability parameters that produced a “combined best fit” to the experimental water transport data at two or more cooling rates, the nonlinear curve fitting code was slightly modified such that  $R^2$  was minimized by one set of parameters for all cooling rates as previously described (Smith *et al* 1998, Devireddy *et al* 1999(b), Devireddy *et al* 2000, Devireddy *et al* 2002).

All the curve fitting results presented have an  $R^2$  value greater than or equal to 0.98 indicating that there was a good agreement between the experimental data points and the fit calculated using the estimated membrane permeability parameters. To simulate the biophysical response of a sperm cell under a variety of cooling rates the best fit parameters were substituted in the water transport equation which was then numerically solved using a 4th order Runge-Kutta

method using a FORTRAN code on a Mac Powerbook G4 (Apple Computer Inc, Cupertino, CA) workstation.

### 3.4 Results

#### 3.4.1 Dynamic Cooling Response and Membrane Permeability Parameters

Fig 3.1 shows the water transport data and simulation using best fit parameters in Eqn. 3.3 at cooling rates of 5 and 10°C/min in the skim milk semen extender (in the absence of CPAs). The open (○) and filled (●) circles represent the DSC water transport (volumetric shrinkage) data at the cooling rate of 5 and 10 °C/min, respectively. The dynamic portion of the cooling curve is between -0.53 °C to -8 °C at these cooling rates. Water transport cessation is observed in the DSC heat release data as an overlap of the thermograms from the heat release signature obtained using osmotically active (initial) and inactive (final) cells, as seen in Fig 1.4 (main introduction). The best fit of Eqn. (3.3) to the 5 °C/min water transport data was obtained for membrane permeability parameter values of  $L_{pg} = 0.68 \times 10^{-15} \text{ m}^3/\text{Ns}$  (0.004  $\mu\text{m}/\text{min-atm}$ ) and  $E_{Lp} = 109.9 \text{ kJ/mole}$  (26.3 kcal/mole) with an  $R^2$  value of 0.99, while the corresponding values for the 10 °C/min data are  $L_{pg} = 0.51 \times 10^{-15} \text{ m}^3/\text{Ns}$  (0.003  $\mu\text{m}/\text{min-atm}$ ) and  $E_{Lp} = 58.5 \text{ kJ/mole}$  (14.0 kcal/mole) with an  $R^2$  value of 0.98 (Table 3.1). A new set of membrane permeability parameters ( $L_{pg}$  and  $E_{Lp}$  or  $L_{pg} [cpa]$  and  $E_{Lp} [cpa]$ ) were obtained that produced a “combined best fit” to the experimentally determined water transport data in the skim milk extender, as shown in Table 3.1. The “combined best fit” membrane permeability parameters maximized the goodness of fit parameter,  $R^2$ , for the 5 and 10 °C/min water transport data concurrently, as described in earlier studies (Smith *et al* 1998, Devireddy *et al* 1999(b), Devireddy *et al* 2000, Devireddy *et al* 2002). The “combined best fit” parameters compare quite closely with the parameters obtained at the higher cooling rate of 10 °C/min, presumably due to

the fact that the 10 °C/min water transport data is farther away from equilibrium than the 5 °C/min data (Smith *et al* 1998, Devireddy *et al* 1999(b), Devireddy *et al* 2000, Devireddy *et al* 2002). The fits generated by the combined best fit parameters are shown in Fig 3.1 as solid lines (——).

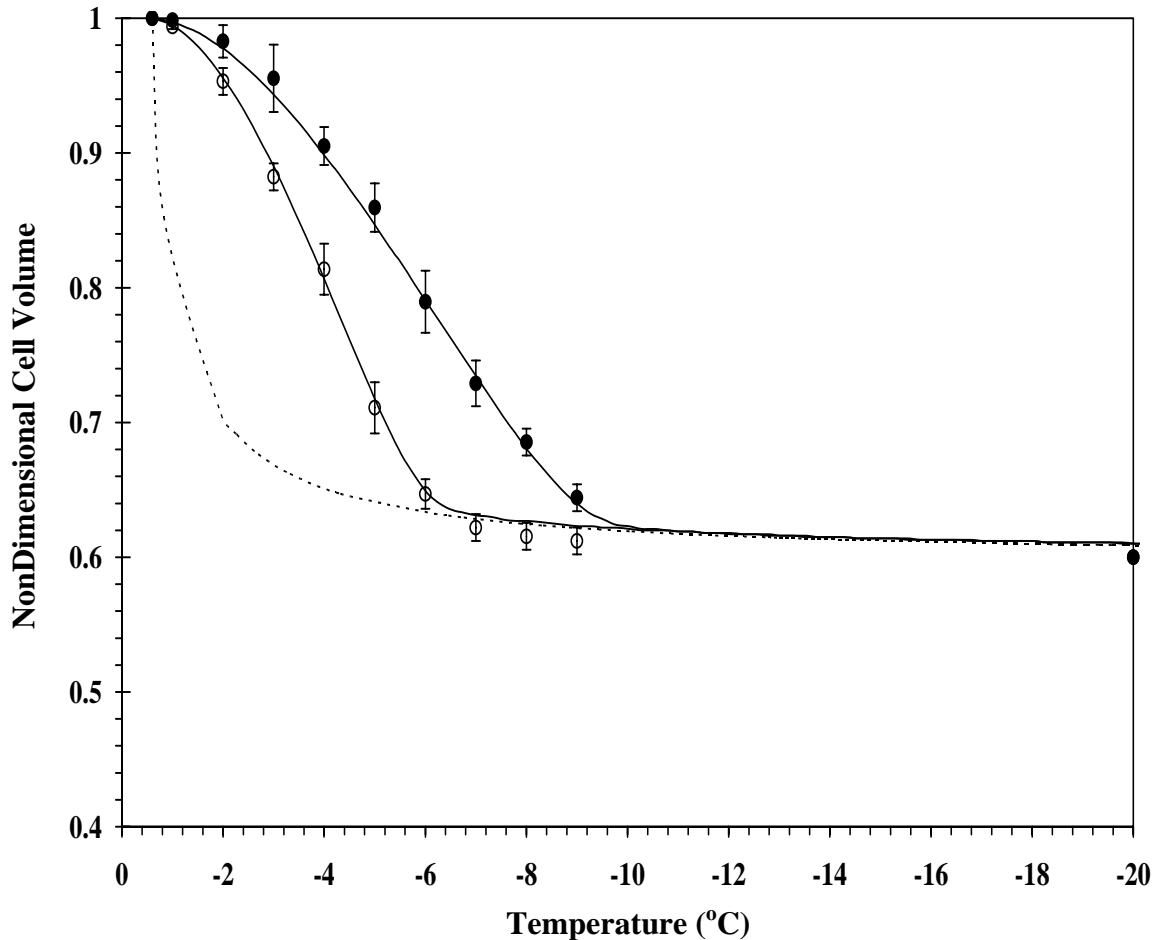


Figure 3.1. Volumetric response of canine sperm cells as a function of subzero temperatures obtained using the DSC technique in the presence of extracellular ice but in the absence of CPAs. The open (○) and filled (●) circles represent the dynamic water transport data at 5 and 10 °C/min respectively. The model simulated dynamic cooling response at 5 and 10 °C/min is shown as a solid line (——) and was obtained by using the “combined best fit” membrane permeability parameters ( $L_{pg}$  and  $E_{Lp}$ ) shown in Table 3.1, in the water transport equation (Eqns. 15 and 16). The model simulated equilibrium cooling response obtained is shown as a dotted line (-----). The nondimensional volume is plotted along the y-axis and the subzero temperatures are shown along the x-axis. The error bars represent the standard deviation in the data (n = 6 separate DSC experiments).

The model simulated equilibrium cooling response<sup>2</sup> is also shown for reference as (-----) and is generated by setting the left hand side (LHS) of Eqn. 3.3 = 0 and balancing the intracellular and extracellular unfrozen chemical activity of water on the right hand side (RHS) at a particular subzero temperature.

Table 3.1: Predicted Sub-Zero Membrane Permeability Parameters for Canine Sperm Cells in the Presence of Extracellular Ice

<i>Cooling Rate</i> (°C/min)	$L_{pg}$ or $L_{pg}$ [cpa] x 10 <sup>15</sup> m <sup>3</sup> /Ns (μm/min-atm)	$E_{Lp}$ or $E_{Lp}$ [cpa] kJ/mol (kcal/mole)	$R^2$ Value
5	0.61 (0.0036)	109.9 (26.3)	0.986
10	0.49 (0.0029)	58.5 (14.0)	0.984
<b>CBF<sup>a</sup></b>	<b>0.49 (0.0029)</b>	<b>63.9 (15.3)</b>	<b>0.987</b>

<sup>a</sup>The combined best fit (CBF) parameters minimized the  $R^2$  value, concurrently, at both 5 and 10 °C/min.

Fig 3.2 shows the water transport data and simulation using the combined best fit parameters in Eqn. 3.3 at cooling rates of 5 and 10 °C/min in the presence of glycerol as the CPA. Figs 3.2A, 3.2B and 3.2C show the measured water transport data in the presence of 0.5%, 3% and 6% glycerol respectively. In all the figures, the open (○) and filled (●) circles represent water transport data at the cooling rates of 5 and 10 °C/min, respectively. The dynamic portion of the cooling curve at these cooling rates is found to be between -0.7 °C to -8 °C in the presence of 0.5% glycerol, between -1.3 °C and -12 °C in the presence of 3% glycerol and

---

<sup>2</sup> Equilibrium is achieved at each temperature when the internal and external osmotic pressures are equal (i.e.  $\pi_i = \pi_o$ ).

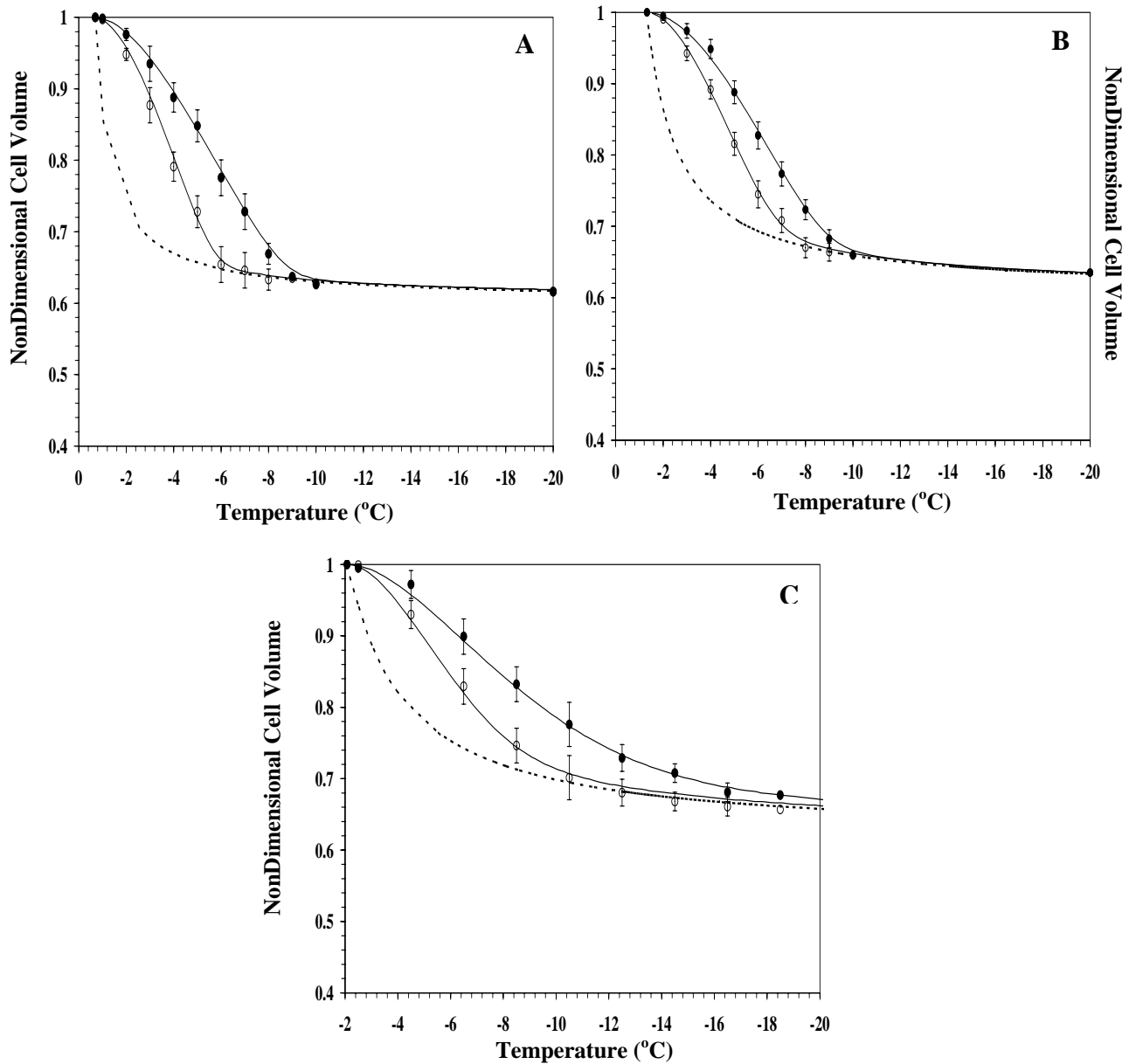


Figure 3.2: Volumetric response of canine sperm cells as a function of subzero temperatures obtained using the DSC technique in the presence of extracellular ice and in the presence of glycerol as a cryoprotective agent. Figs 3.2A, 3.2B and 3.2C represent water transport data obtained in the presence of 0.5%, 3% and 6% glycerol in skim milk extender, respectively. In all the figures, the open ( $\circ$ ) and filled ( $\bullet$ ) circles represent the dynamic water transport data at 5 and 10  $^{\circ}\text{C}/\text{min}$  respectively. The model simulated dynamic cooling response at 5 and 10  $^{\circ}\text{C}/\text{min}$  is shown as a solid line (—) and was obtained by using the “combined best fit” membrane permeability parameters ( $L_{pg}$  and  $E_{Lp}$ ) shown in Table 3.2, in the water transport equation (Eqns. 3.3 and 3.4). The model simulated equilibrium cooling response obtained is shown as a dotted line (-----) in all the figures. The nondimensional volume is plotted along the y-axis and the subzero temperatures are shown along the x-axis. The error bars represent the standard deviation in the data ( $n = 6$  separate DSC experiments).

between  $-2.1\text{ }^{\circ}\text{C}$  and  $14\text{ }^{\circ}\text{C}$  in the presence of 6% glycerol, as shown in Figs 3.2A, 3.2B and 3.2C respectively. The best fit parameter values of  $L_{pg}[cpa]$  and  $E_{Lp}[cpa]$  are shown in Table 3.2 along with the combined best fit values of  $L_{pg}[cpa]$  and  $E_{Lp}[cpa]$  in the presence of extracellular ice and glycerol. The fits generated by the combined best fit parameters are shown in Fig 3.2 as solid lines (——) and the model simulated equilibrium cooling response is also shown for reference as (-----)

Table 3.2. Predicted Sub-Zero Membrane Permeability Parameters for Canine Sperm Cells in the Presence of Extracellular Ice and Glycerol:

<i>Concentration of Glycerol (v/v)</i>	<i>Cooling Rate (<math>^{\circ}\text{C}/\text{min}</math>)</i>	$L_{pg}$ or $L_{pg}[cpa]$ x $10^{15}$ m <sup>3</sup> /Ns ( $\mu\text{m}/\text{min-atm}$ )	$E_{Lp}$ or $E_{Lp}[cpa]$ kJ/mol (kcal/mole)	$R^2$ Value
0.5%	5	0.56 (0.0033)	82.4 (19.7)	0.986
	10	0.51 (0.003)	54.33 (13.0)	0.986
	<b>CBF<sup>a</sup></b>	<b>0.51 (0.003)</b>	<b>56.0 (13.4)</b>	<b>0.986</b>
3.0%	5	0.51 (0.003)	61.0 (14.6)	0.976
	10	0.51 (0.003)	43.1 (10.3)	0.977
	<b>CBF<sup>a</sup></b>	<b>0.51 (0.003)</b>	<b>46.4 (11.1)</b>	<b>0.977</b>
6.0%	5	0.51 (0.003)	99 (23.9)	0.990
	10	0.94 (0.0055)	130.8 (31.3)	0.990
	<b>CBF<sup>a</sup></b>	<b>0.85 (0.005)</b>	<b>121.2 (29.0)</b>	<b>0.990</b>

<sup>a</sup>The combined best fit (CBF) parameters minimized the  $R^2$  value, concurrently, at both 5 and 10  $^{\circ}\text{C}/\text{min}$ .

Fig 3.3 shows the water transport data and simulation using best fit parameters in Eqn. 3.3 at cooling rates of 5 and 10 $^{\circ}\text{C}/\text{min}$  in the presence of dimethylsulfoxide as the CPA. Figs

3.3A and 3.3B show the measured water transport data in the presence of 0.5% and 3% dimethylsulfoxide respectively. In both the figures, the open ( $\circ$ ) and filled ( $\bullet$ ) circles represent water transport data at the cooling rates of 5 and 10 °C/min, respectively. The dynamic portion of the cooling curve at these cooling rates is found to be between -0.7 °C to -8 °C in the presence

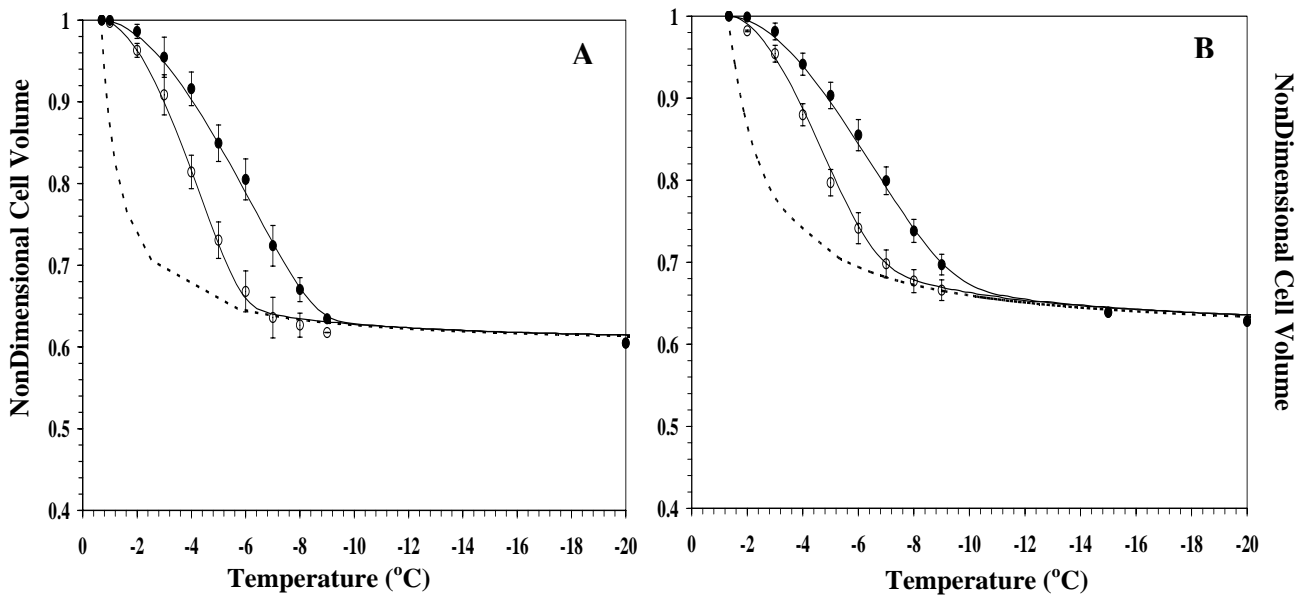


Figure 3.3. Volumetric response of canine sperm cells as a function of subzero temperatures obtained using the DSC technique in the presence of extracellular ice and in the presence of dimethylsulfoxide as a cryoprotective agent. Figs 3.3A and 3.3B represent water transport data obtained in the presence of 0.5% and 3% dimethylsulfoxide in skim milk extender, respectively. In all the figures, the open ( $\circ$ ) and filled ( $\bullet$ ) circles represent the dynamic water transport data at 5 and 10 °C/min, respectively. The model simulated dynamic cooling response at 5 and 10 °C/min is shown as a solid line (—) and was obtained by using the “combined best fit” membrane permeability parameters ( $L_{pg}$  and  $E_{Lp}$ ) shown in Table 3.3, in the water transport equation (Eqns. 15 and 16). The model simulated equilibrium cooling response obtained is shown as a dotted line (-----) in both the figures. The nondimensional volume is plotted along the y-axis and the subzero temperatures are shown along the x-axis. The error bars represent the standard deviation in the data ( $n = 6$  separate DSC experiments).

of 0.5% dimethylsulfoxide and between -1.3 °C and -12 °C in the presence of 3% dimethylsulfoxide, as shown in Figs 3.3A and 3.3B respectively. The best fit parameter values of  $L_{pg}$  [cpa] and  $E_{Lp}$  [cpa] are shown in Table 3.3 along with the combined best fit values

of  $L_{pg}[cpa]$  and  $E_{Lp}[cpa]$  in the presence of extracellular ice and dimethylsulfoxide. The fits generated by the combined best fit parameters are shown in Fig 3.3 as solid lines (——) and the model simulated equilibrium cooling response is also shown for reference as (-----)

### 3.4.2 Statistical Analysis

The DSC water transport data at 5 and 10 °C/min were found to be statistically significantly different from one another with  $\geq 95\%$  confidence level (in the dynamic part of the cooling curve) in all the media combinations investigated. However, the differences in the water transport data obtained using glycerol and dimethylsulfoxide at corresponding concentrations (i.e. comparing water transport data obtained with 0.5% glycerol and 0.5% dimethylsulfoxide and at the higher concentration of 3%) were found to be statistically significant only with  $\geq 80\%$  confidence level (at both 5 and 10 °C/min, in the dynamic part of the cooling curve). This suggests that the effect of glycerol and dimethylsulfoxide on the canine sperm permeability parameters is similar, if not exactly the same. The differences in the water transport data when compared across concentrations of CPA (i.e. comparing the water transport data obtained using 0.5% glycerol with either 3.0% glycerol or 3.0% dimethylsulfoxide and for other similar combinations) were found to be statistically significant with a confidence level  $\geq 95\%$  (at both 5 and 10 °C/min). And finally, the differences in the water transport data obtained in the absence and in the presence of CPA were found to be statistically significant with a confidence level  $\geq 95\%$  (at both 5 and 10 °C/min).

Table 3.3. Predicted Sub-Zero Membrane Permeability Parameters for Canine Sperm Cells in the Presence of Extracellular Ice and Dimethylsulfoxide (Me<sub>2</sub>SO)

<i>Concentration of Dimethylsulfoxide (v/v)</i>	<i>Cooling Rate (°C/min)</i>	$L_{pg}$ or $L_{pg}$ [cpa] x 10 <sup>15</sup> m <sup>3</sup> /Ns ( $\mu$ m/min-atm)	$E_{Lp}$ or $E_{Lp}$ [cpa] kJ/mol (kcal/mole)	$R^2$ Value
0.5%	5	0.56 (0.0033)	98.2 (23.5)	0.986
	10	0.46 (0.0027)	54.8 (13.1)	0.978
	<b>CBF<sup>a</sup></b>	<b>0.46 (0.0027)</b>	<b>54.8 (13.1)</b>	<b>0.984</b>
3.0%	5	0.68 (0.004)	74.8 (17.9)	0.980
	10	0.48 (0.0028)	46.8 (11.2)	0.973
	<b>CBF<sup>a</sup></b>	<b>0.51 (0.003)</b>	<b>51.4 (12.3)</b>	<b>0.975</b>

<sup>a</sup>The combined best fit (CBF) parameters minimized the  $R^2$  value, concurrently, at both 5 and 10 °C/min.

### 3.4.3 Combined Best Fit Parameters

As stated earlier, a new set of membrane permeability parameters ( $L_{pg}$  and  $E_{Lp}$  or  $L_{pg}$  [cpa] and  $E_{Lp}$  [cpa]) were obtained that produced a “combined best fit” to the experimentally determined water transport data. The “combined best fit” membrane permeability parameters maximized the goodness of fit parameter,  $R^2$ , for the 5 and 10 °C/min water transport data concurrently. Fig 3.4 shows the contour plots of the goodness of fit parameter,  $R^2$  (= 0.95) in the  $L_{pg}$  and  $E_{Lp}$  (or  $L_{pg}$  [cpa] and  $E_{Lp}$  [cpa]) space that “fit” the water transport data at 5 and 10 °C/min in the skim milk extender without CPAs (Fig 3.4A) and in the freezing media containing 0.5% glycerol (Fig 3.4B), 3.0% glycerol (Fig 3.4C) and 6.0% glycerol (Fig 3.4D), respectively. Any combination of  $L_{pg}$  and  $E_{Lp}$  (or  $L_{pg}$  [cpa] and  $E_{Lp}$  [cpa]) shown to be within the contour will

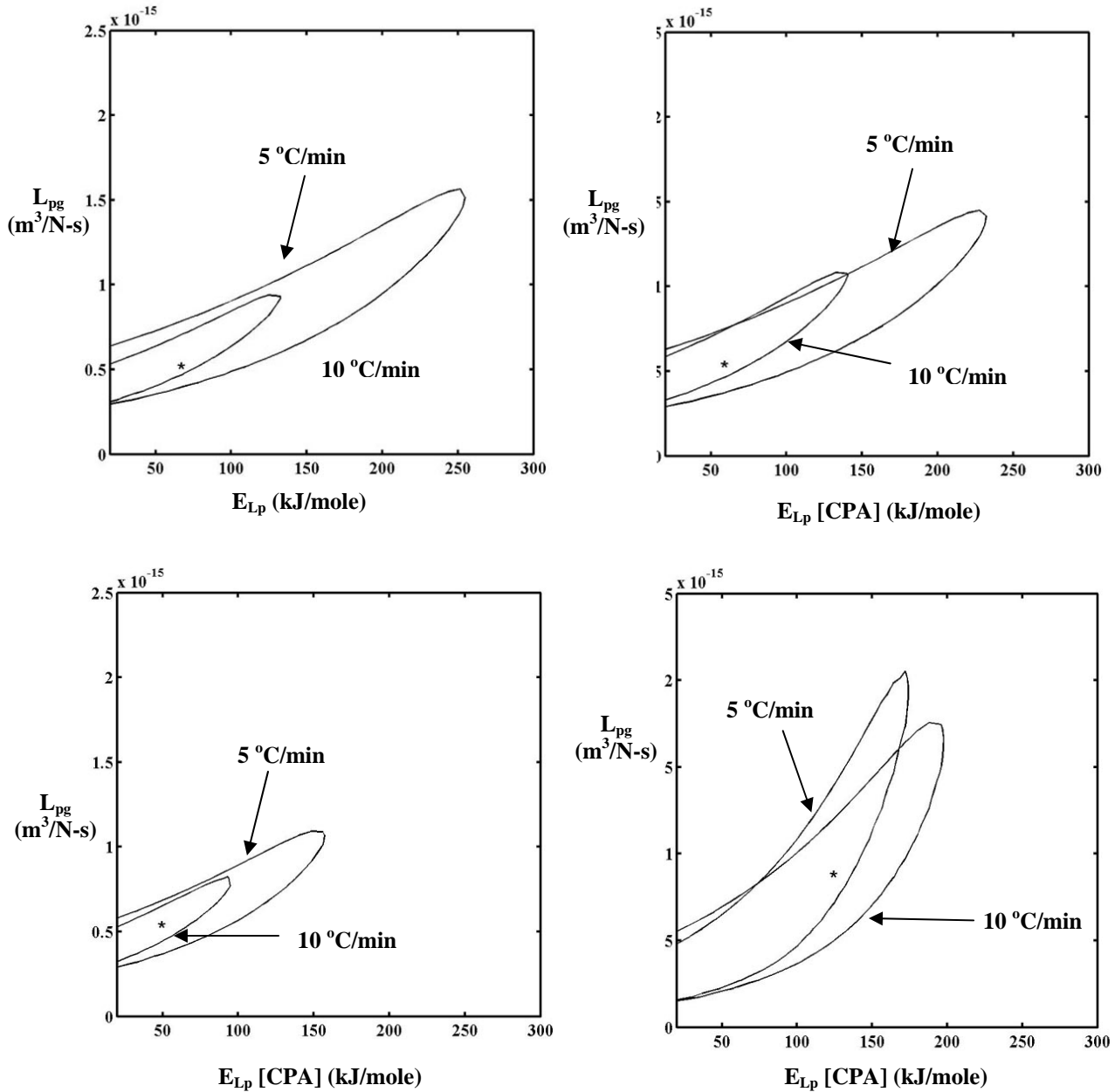


Figure 3.4. Contour plots of the goodness of fit parameter  $R^2$  ( $= 0.95$ ) for water transport response in sperm cells in skim milk extender (Fig 3.4A) and in solutions with 0.5% (Fig 3.4B), 3% (Fig 3.4C) and 6% glycerol (Fig 3.4D). The common region corresponds to the range of parameters that “fit” the water transport data at both the cooling rate (either 5 or 10 °C/min) with  $R^2 \geq 0.95$ . Note that the “combined best fit” parameters are represented by a “\*” in all the figures. The membrane permeability at 0 °C,  $L_{pg}$  (or  $L_{pg} [cpa]$ ) ( $m^3/Ns$ ) is plotted on the y-axis while the apparent activation energy of the membrane,  $E_{Lp}$  (or  $E_{Lp} [cpa]$ ) (kJ/mole) is plotted on the x-axis.

“fit” the water transport data at that cooling rate with an  $R^2$  value  $> 0.95$ . In Skim Milk Extender (See Fig 3.4A), the “combined best fit” parameters are,  $L_{pg} = 0.49 \times 10^{-15} \text{ m}^3/\text{Ns}$  (0.0029  $\mu\text{m}/\text{min-atm}$ ) and  $E_{Lp} = 63.9 \text{ kJ/mole}$  (15.3 kcal/mole). For media with 0.5% glycerol (See Fig. 3.4B), the “combined best fit” parameters are,  $L_{pg}[cpa] = 0.51 \times 10^{-15} \text{ m}^3/\text{Ns}$  (0.003  $\mu\text{m}/\text{min-atm}$ ) and  $E_{Lp}[cpa] = 56.0 \text{ kJ/mole}$  (13.4 kcal/mole), where as for media with 3% glycerol (See Fig. 3.4C), the “combined best fit” parameters are,  $L_{pg}[cpa] = 0.51 \times 10^{-15} \text{ m}^3/\text{Ns}$  (0.003  $\mu\text{m}/\text{min-atm}$ ) and  $E_{Lp}[cpa] = 46.4 \text{ kJ/mole}$  (11.1 kcal/mole). Fig 3.4D represents contour plots for media with 6% glycerol. The “combined best fit” parameters for 6% glycerol are,  $L_{pg}[cpa] = 0.85 \times 10^{-15} \text{ m}^3/\text{Ns}$  (0.005  $\mu\text{m}/\text{min-atm}$ ) and  $E_{Lp}[cpa] = 121.2 \text{ kJ/mole}$  (29.0 kcal/mole).

Note that the contours for the higher cooling rate of 10 °C/min are smaller than those obtained at the lower cooling rate of 5 °C/min. This suggests that the membrane permeability parameters obtained using the 10 °C/min water transport data could predict the volumetric response of the sperm cell at the lower cooling rate of 5 °C/min quite accurately, while the converse is not true. Therefore, to obtain the membrane permeability parameters that “best predict” the behavior of a biological system, water transport data needs to be obtained at the highest possible cooling rate at which dehydration occurs exclusively (Smith *et al* 1998, Devireddy *et al* 1999(b), Devireddy *et al* 2000, Devireddy *et al* 2002, Devireddy *et al* 2003).

### 3.4.4 Water Transport Simulations

Water transport simulations obtained using the “combined best fit” parameters in Eqn. 3.3 are shown for a variety of cooling rates (5 - 100 °C/min) in Fig. 3.5. In Figs 3.5A, 3.5B, 3.5C, 3.5D, 3.5E and 3.5F, the numerically simulated nondimensional cellular volume ( $V/V_0$ ) obtained using

the “combined best fit” parameters (taken from Tables 3.1, 3.2 and 3.3) is shown for a variety of cooling rates (at 5, 10, 20, 40, 50 and 100 °C/min) in the skim milk extender, in the media containing 0.5% glycerol, 3.0% glycerol, 6.0% glycerol, 0.5% dimethylsulfoxide and 3.0% dimethylsulfoxide, respectively. The nondimensional cellular volume ( $V/V_0$ ), which decreases due to dehydration during freezing, is plotted on the y-axis while the sub zero temperatures are plotted on the x-axis. From the simulations, the amount of trapped water (or a lower boundary on the intracellular ice) was computed as a ratio of the volume of the water trapped inside the sperm cell at the temperature,  $T$  ( $\sim -30$  °C) where intracellular ice formation can occur by a homogenous or volume catalyzed nucleation (Karlsson *et al* 1993, Karlsson *et al* 1994, Toner 1993) to the initial sperm water volume,  $[(V-V_b)/(V_0-V_b)]$  as described earlier for a several biological systems, including the rat liver tissue system (Devireddy *et al* 1999(b), Devireddy and Bischof 2003), mouse (Devireddy *et al* 1999(a)), human (Devireddy *et al* 2000) and horse sperm (Devireddy *et al* 2002) cells<sup>3</sup>. In the absence of CPAs, for cooling rates of  $\leq 20, 40, 50$  and  $100$  °C/min, the trapped water volume was  $\leq 2.5\%, 6.5\%, 23.0\%$  and  $60.5\%$  of the initial osmotically active water volume, respectively, and the corresponding end volumes were  $\leq 0.61V_0, 0.626V_0, 0.692V_0$  and  $0.842V_0$ , respectively (Fig 3.5A). Similar analysis was performed for all the media combinations shown in Figs 3.5B to 3.5F (data not shown). In the interest of brevity, corresponding end volume and % of initial water trapped data is presented only for one other CPA media combination: 3% glycerol (Fig 3.5C). In the presence of 3% glycerol (Fig 3.5C), for cooling rates of  $\leq 20, 40, 50$  and  $100$  °C/min, the trapped water volume was  $\leq 3.9\%, 6.9\%$ ,

---

<sup>3</sup>Where  $V$  is the end volume after water transport ceases (at  $\sim -30$  °C), and  $V_0$  and  $V_b$  are the initial (isotonic) and final (osmotically inactive) sperm cell volumes, respectively

13.3% and 52.1% of initial osmotically active water volume, respectively,  $\leq 0.635V_0$ ,  $0.637V_0$ ,  $0.662V_0$  and  $0.813V_0$ , respectively.

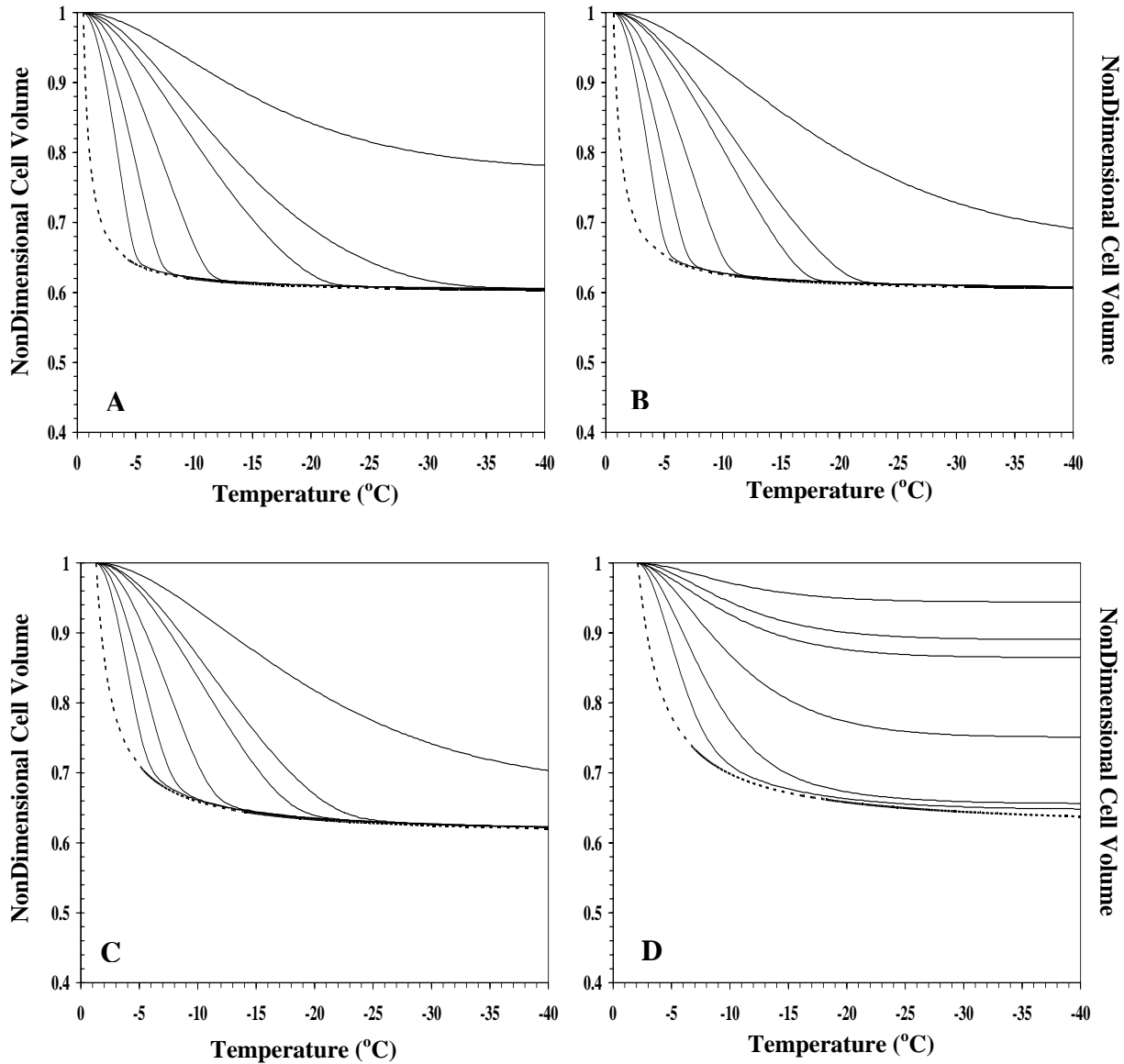


Figure 3.5: Volumetric response of canine sperm cells at various cooling rates as a function of subzero temperatures using the “combined best fit” membrane permeability parameters (shown in Tables 3.1, 3.2 and 3.3).

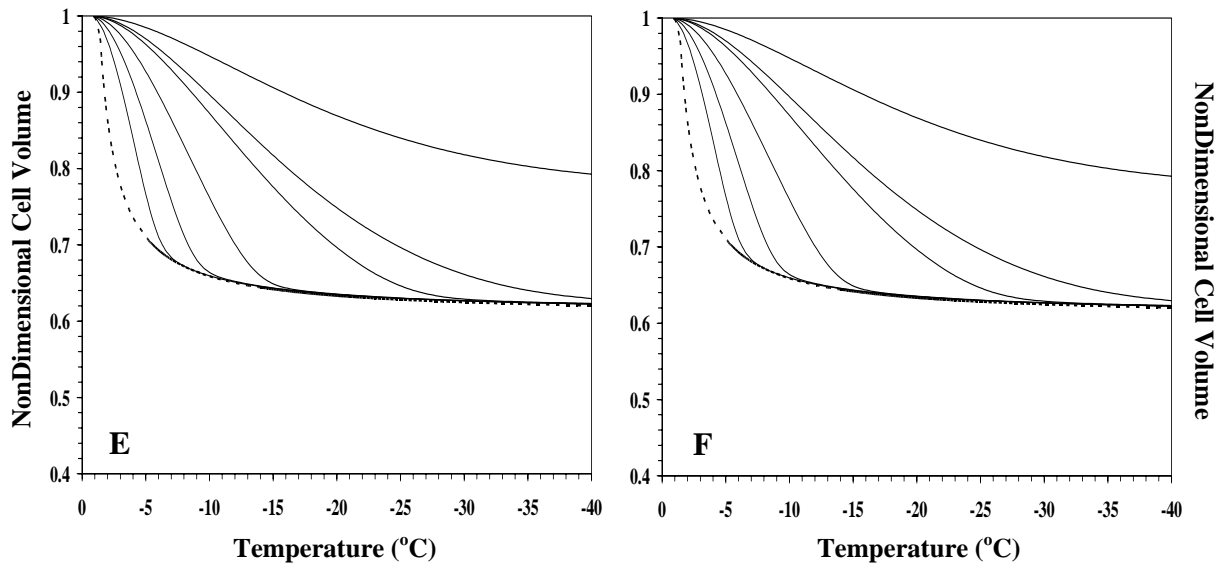


Figure 3.5 Continued: Figures 5A, 5B, 5C, 5D, 5E and 5F show the changes in the normalized cell volume ( $V/V_0$ ) as a function of temperature for different cooling rates in skim milk extender, in skim milk extender + 0.5% glycerol, in skim milk extender + 3.0% glycerol, in skim milk extender + 6.0% glycerol, in skim milk extender + 0.5% dimethylsulfoxide and in skim milk extender + 0.5% dimethylsulfoxide, respectively. The water transport curves (—) plotted in Fig. 6 represent the model simulated response for different cooling rates (from left to right: 5, 10, 20, 40, 50 and 100 °C/min) using the combined best fit parameters shown in Tables 3.1, 3.2 and 3.3. The model simulated equilibrium cooling response is also shown in all the figures as a dotted line (-----). The subzero temperatures are shown along the x-axis while the nondimensional volume is plotted along the y-axis.

As described earlier (see Introduction), the cooling rate which optimizes the freeze/thaw response of any cellular system can be defined as the fastest cooling rate in a given media without forming damaging intracellular ice formation, IIF (Mazur 1972). Mazur (1990) defines IIF as damaging and lethal if > 10-15% of the initial intracellular water is involved. We defined the “optimal cooling rate” as the cooling rate at which 5% of the initial osmotically active water volume is trapped inside the cells at temperature,  $T \sim -30^\circ\text{C}$ . The simulations (shown in Fig. 3.5) obtained using the combined best fit parameters show that the “optimal cooling rate” in the absence of CPAs, in the media containing 0.5% glycerol, 3.0% glycerol, 6.0% glycerol, 0.5% dimethylsulfoxide and 3.0% dimethylsulfoxide are 26.6, 32.6, 31.8, 9.2, 29.4 and 29.2 °C/min,

respectively. Note, that if intracellular ice formation (IIF) occurs by a heterogeneous or a surface catalyzed nucleation mechanism (Toner 1993) (generally between -5 and -20 °C for a variety of single cells), which our model does not predict, then potentially even more water will be trapped in the sperm cells than predicted by water transport alone (i.e. the lower boundary of intracellular ice discussed above). Thus, the “optimal cooling rates” (stated above) based on the lower boundary of intracellular ice are probably over estimated.

### **3.5 Discussion**

#### **3.5.1 Effect of Cooling Rate on Predicted Membrane Permeability Parameters**

There is a significant decrease (~20 - 50%) in the predicted value of the activation energy,  $E_{Lp}$  (or  $E_{Lp} [cpa]$ ) between the 5 and 10 °C/min DSC water transport data (Tables 3.1, 3.2 and 3.3). It might be that the sperm cells cooled at 10 °C/min undergo incomplete dehydration and the final end volume is significantly higher than the osmotically inactive cell volume of  $0.6V_0$  or that the sperm cells experience intracellular ice formation, IIF when cooled at 10 °C/min. Unfortunately, at the present time, we have no independent means of verifying the end volumes for canine sperm cells cooled at 10 °C/min to -20 °C. However, it should be pointed out that a similar drop in predicted value of the activation energy,  $E_{Lp}$  (or  $E_{Lp} [cpa]$ ) was also found in normal rat hepatocyte cells both in the presence and absence of CPA (dimethylsulfoxide, DMSO) using standard cellular cryomicroscopy (Smith *et al* 1998), in Dunning AT-1 rat prostate tumor tissue (Devireddy *et al* 1999(b)) as well in several mammalian sperm cells (Devireddy *et al* 1999(a), Devireddy *et al* 2000, Devireddy *et al* 2002) using the DSC technique. In addition, the viability/motility results obtained by Yu *et al* (2002) suggest that significant IIF is not occurring at 10 °C/min, as the percent viability/motility increases or remains constant between < 10 °C/min and 10 °C/min (i.e. reflects “solute effects” as the

dominant mechanism of freezing injury and not IIF). This suggests that water transport is still the dominant biophysical response in canine sperm cells cooled at 10 °C/min. This is further supported by the observation that, a) the magnitude of the DSC measured difference in heat release,  $\Delta q_{dsc}$ , was found to be constant between 5 and 10 °C/min; and b) no secondary heat release was observed at 10 °C/min to suggest incomplete dehydration, as was the case for EBVT lymphocytes (Devireddy *et al* 1998), liver tissue of a freeze tolerant wood frog (Devireddy *et al* 1999(c)). Therefore, for the purpose of this study it was assumed that the sperm cells undergo complete dehydration to the osmotically inactive cell volume of  $0.6V_0$  at a cooling rate of 10 °C/min. The observed change in the activation energy is assumed to be intrinsic to the water transport data itself; where more information is contained in data from cooling rates further away from equilibrium cooling, i.e. 10 °C/min water transport data contains more dynamic information than at 5 °C/min, as noted earlier (Smith *et al* 1998, Devireddy *et al* 1999 (b)).

### **3.5.2 Experiments at Higher Cooling Rates**

As noted earlier and in other studies, it is essential that water transport parameters be obtained at the highest possible cooling rate at which dehydration occurs exclusively (Smith *et al* 1998, Devireddy *et al* 1999(b), Devireddy *et al* 2000, Devireddy *et al* 2002, Devireddy *et al* 2003). One of the main disadvantages of the DSC technique is that it cannot distinguish between the heat releases obtained during water transport and IIF, so a correlative method is needed to determine that the biophysical response is in fact water transport and not IIF (Devireddy *et al* 1999(b)). Since standard cellular cryomicroscopy cannot be used to determine the biophysical response during freezing in canine sperm, an indirect methodology was used to determine the maximum cooling rate at which water transport occurs exclusively in human sperm. Yu *et al.* (2002) report that the plot of motility and the membrane integrity versus

cooling rate resembles an inverted “U” curve with an optimal cooling rate of 10 °C/min (with either rapid or slow thawing rates) in the presence of 0.6 Osm glycerol. These data suggest that the loss of motility, plasma membrane integrity and mitochondrial function at cooling rates > 10 °C/min is due to the formation of IIF. Thus, the highest cooling rate which causes water transport to occur exclusively in canine sperm in the presence of 0.6 Osm glycerol (which is within the range of the concentration of glycerol used in this study, 0.07 Osm to 0.84 Osm) is ~10 °C/min and hence DSC experiments were not performed at higher cooling rates. It is possible that in the absence of CPA, some IIF may occur at 10 °C/min. However, for the purpose of this study this possibility was considered negligible.

### **3.5.3 Parameter Sensitivity Analysis - Effect of Varying the Osmotically Inactive Cell Volume ( $V_b$ )**

The value of the osmotically inactive cell volume of canine and other mammalian sperm cells has been reported to be ranging from  $0.6V_0$  (the value used in this and other studies) to as low  $0.23V_0$  and as high as  $\sim 0.75V_0$  (Kleinhans *et al* 1992, Gilmore *et al* 1995, Gilmore *et al* 1996, Goa *et al* 1997, Gilmore *et al* 1998, Devireddy *et al* 1999(b), Devireddy *et al* 2000, Devireddy *et al* 2002, Devireddy *et al* 2003). To study the effect of varying the osmotically inactive cell volume on the predicted membrane permeability parameters ( $L_{pg}$  and  $E_{LP}$ ), the value of  $V_b$  was increased to  $0.8V_0$  and decreased to  $0.4V_0$ . The DSC data was correspondingly modified (using Eqn. 1.2) and the modified DSC water transport data was curve fitted to the water transport model (Eqns. 3.3 and 3.4) using the nonlinear least squares curve fitting technique as previously described. The predicted values of the membrane permeability parameters ( $L_{pg}$  and  $E_{LP}$ ; in the interest of brevity only values obtained in the absence of any CPA and in the presence of glycerol are shown) using a value of  $0.4V_0$  as the osmotically inactive cell

volume are shown in Table 3.4 while the corresponding values obtained using a value of  $0.8V_o$  are shown in Table 3.5. A decrease of  $\sim 33\%$  in the value of  $V_b$  from  $0.6V_o$  to  $0.4V_o$  results in the model predicted membrane permeability parameters to be within 20% of each other (as shown in Tables 3.1, 3.2, 3.3 and 3.4). Similarly, an increase of 33% in the value of  $V_b$  from  $0.6V_o$  to  $0.8V_o$  results in the model predicted membrane permeability parameters to be within 15% of each other (as shown in Tables 3.1, 3.2, 3.3 and 3.5). This lack of sensitivity in the membrane permeability parameters to the value of the osmotically inactive cell volume has been reported in the literature for a variety of cell and tissue systems (Smith *et al* 1998, Devireddy *et al* 1999(b), Devireddy *et al* 2000, Devireddy *et al* 2002, Devireddy *et al* 2003). Thus, errors in the estimated value of  $V_b$  can alter the model predicted membrane permeability parameters ( $L_{pg}$  and  $E_{Lp}$ ) but the trends remain the same.

The effect of varying the osmotically inactive cell volume on the model simulated value of trapped water (or a lower boundary on intracellular ice) was also investigated. This was done by performing additional water transport simulations using the “combined best fit” parameters shown in Tables 3.4 and 3.5. The predicted optimal cooling rates obtained using the parameters shown in Tables 3.4 and 3.5 are in very good agreement ( $\pm 5\%$ ) to that obtained using the values of the membrane permeability parameters shown in Tables 3.1 to 3.3 (data not shown). Thus, the variation in the value of  $V_b$  doesn't significantly alter the model predictions and as noted earlier depending on the concentration of CPAs, cooling rates as low as 10 to 30 °C/min can cause a significant amount of intracellular water to be trapped inside the canine spermatozoa.

Table 3.4: Predicted Sub-Zero Membrane Permeability Parameters for Canine Sperm Cells in the Presence of Extracellular Ice and CPAs assuming  $V_b = 0.4V_o$

<i>Freezing Media</i>	<i>Cooling Rate</i> (°C/min)	$L_{pg}$ or $L_{pg}$ [cpa] x 10 <sup>15</sup> m <sup>3</sup> /Ns ( $\mu\text{m}/\text{min-atm}$ )	$E_{Lp}$ or $E_{Lp}$ [cpa] kJ/mol (kcal/mole)	$R^2$ Value
<b>Skim Milk Extender (No CPA)</b>	5	0.77 (0.0045)	109.1 (26.1)	0.986
	10	0.48 (0.0028)	69.8 (16.7)	0.980
	<b>CBF<sup>a</sup></b>	<b>0.51(0.003)</b>	<b>65.2 (15.6)</b>	<b>0.986</b>
<b>Skim Milk Extender + 0.5% Glycerol</b>	5	0.58(0.0034)	75.7 (18.1)	0.986
	10	0.60(0.0035)	55.6 (13.3)	0.986
	<b>CBF<sup>a</sup></b>	<b>0.60 (0.0035)</b>	<b>52.3 (12.5)</b>	<b>0.987</b>
<b>Skim Milk Extender + 3.0% Glycerol</b>	5	0.65(0.0038)	53.1 (12.7)	0.978
	10	0.54 (0.0032)	43.9 (10.5)	0.977
	<b>CBF<sup>a</sup></b>	<b>0.51 (0.003)</b>	<b>50.6 (12.1)</b>	<b>0.977</b>
<b>Skim Milk Extender + 6.0% Glycerol</b>	5	0.51(0.0030)	92.8 (22.2)	0.991
	10	0.90(0.0053)	130.0(31.1)	0.990
	<b>CBF<sup>a</sup></b>	<b>0.87 (0.0051)</b>	<b>115.4 (27.6)</b>	<b>0.988</b>

<sup>a</sup>The combined best fit (CBF) parameters minimized the  $R^2$  value, concurrently, at both 5 and 10 °C/min.

Table 3.5: Predicted Sub-Zero Membrane Permeability Parameters for Canine Sperm Cells in the Presence of Extracellular Ice and CPAs assuming  $V_b = 0.8V_o$

<i>Freezing Media</i>	<i>Cooling Rate</i> (°C/min)	$L_{pg}$ or $L_{pg}$ [cpa] $\times 10^{15} \text{ m}^3/\text{Ns}$ ( $\mu\text{m}/\text{min-atm}$ )	$E_{Lp}$ or $E_{Lp}$ [cpa] kJ/mol (kcal/mole)	$R^2$ Value
<b>Skim Milk Extender (No CPA)</b>	5	0.61 (0.0036)	107.0 (25.6)	0.987
	10	0.46 (0.0027)	66.9(16.0)	0.981
	<b>CBF<sup>a</sup></b>	<b>0.48 (0.0028)</b>	<b>76.1 (18.2)</b>	<b>0.982</b>
<b>Skim Milk Extender + 0.5% Glycerol</b>	5	0.58 (0.0034)	81.5 (19.5)	0.989
	10	0.58 (0.0034)	52.7(12.6)	0.985
	<b>CBF<sup>a</sup></b>	<b>0.58 (0.0034)</b>	<b>60.2(14.4)</b>	<b>0.982</b>
<b>Skim Milk Extender + 3.0% Glycerol</b>	5	0.60(0.0035)	61.0 (14.6)	0.976
	10	0.58 (0.0034)	44.7(10.7)	0.976
	<b>CBF<sup>a</sup></b>	<b>0.60 (0.0035)</b>	<b>49.7(11.9)</b>	<b>0.973</b>
<b>Skim Milk Extender + 6.0% Glycerol</b>	5	0.65(0.0038)	118.3 (28.3)	0.986
	10	1.02(0.006)	132.5 (31.7)	0.987
	<b>CBF<sup>a</sup></b>	<b>1.02 (0.006)</b>	<b>112.9 (27.0)</b>	<b>0.987</b>

<sup>a</sup>The combined best fit (CBF) parameters minimized the  $R^2$  value, concurrently, at both 5 and 10 °C/min.

### 3.5.4 Effect of Extracellular Ice on Membrane Transport Parameters

As mentioned earlier, there are currently no experimental techniques, which yield data on how sperm cells either dehydrate or form intracellular ice during freezing in the presence of extracellular ice (Curry *et al* 1994, Gao *et al* 1997). However, there exist a few techniques like the *Time to Lysis* method (Curry *et al* 1995, Gao *et al* 1997, Noiles *et al* 1993, Noiles *et al* 1995) and *Coulter counter* technique (Gao *et al* 1997, Gilmore *et al* 1995, Gilmore *et al* 1996, Gilmore *et al* 1998) to measure the volumetric response of sperm cells to external changes in osmolarity, at suprazero temperatures. The parameters obtained using these techniques are essentially in agreement; suprazero membrane permeability,  $L_p \sim 0.85 - 17 \times 10^{-13} \text{ m}^3/\text{Ns}$  (0.5 - 10  $\mu\text{m}/\text{min-atm}$ ) and activation energy at suprazero temperatures,  $E_a \sim 12 - 60 \text{ kJ/mol}$  (3 - 14 kcal/mol) and serve to provide a good understanding of suprazero water (and CPA) transport response for a variety of mammalian sperm cells, including human, ram, bull, rabbit and mouse (Gao *et al* 1997). However, these techniques have not as yet been applied to canine sperm and there is a paucity of suprazero permeability parameters for canine sperm.

The extrapolation of the suprazero permeability data obtained in the absence of extracellular ice using the techniques described above to subzero temperatures in the presence of extracellular ice has not been successful (Curry *et al* 1994, Gao *et al* 1997). This conclusion is based on the fact that water permeabilities predicted on the basis of the above mentioned techniques suggest that mammalian sperm cells should be able to dehydrate at rates up to 5000  $^{\circ}\text{C}/\text{min}$  during freezing when in fact experiments show that the “optimal cooling rate” for canine sperm cells is between 10 - 30  $^{\circ}\text{C}/\text{min}$  depending on the concentrations of CPAs in the extracellular milieu (Foote 1964, Hay *et al* 1997, Linde-Forsberg *et al* 1989, Rota *et al* 1999, Yu *et al* 2002). One way to account for this discrepancy is that the values of membrane permeability

parameters at subzero temperatures in the presence of extracellular ice are markedly different than those reported in literature at suprazero temperatures. In particular if  $L_{pg}$  at subzero temperatures is lower by at least an order of magnitude than  $L_p$  at suprazero temperatures and  $E_{Lp}$  at subzero temperatures is higher by at least a factor of two than the corresponding  $E_a$  at suprazero temperatures, then the discrepancy between numerical simulations and experimental data can be reconciled (Curry *et al* 1994, Gao *et al* 1997). The best fit parameters obtained in this study using the DSC water transport data (shown in Tables 3.1 to 3.5), during freezing of canine sperm, confirm that this is indeed the case;  $L_{pg} = 0.46 \times 10^{-15}$  to  $0.53 \times 10^{-15} \text{ m}^3/\text{Ns}$  ( $0.0027$  to  $0.0031 \text{ } \mu\text{m}/\text{min-atm}$ ) and  $E_{Lp} = 46.4$  to  $56.0 \text{ kJ/mole}$  ( $11.1$  to  $13.4 \text{ kcal/mole}$ )

As stated above, the best fit parameters obtained in this study using the DSC water transport data (shown in Tables 3.1 to 3.5) during freezing of canine sperm are significantly lower than the reported suprazero permeability values for other mammalian species (Gao *et al* 1997). A similar dissimilarity was also found for mouse, human and horse sperm cell membrane permeability values (Devireddy *et al* 1999(a), Devireddy *et al* 2000 Devireddy *et al* 2002). This discrepancy between the membrane permeabilities may be associated with possible changes in the sperm cell plasma membrane during suprazero cooling. These changes could include either a lipid phase transition between 0 and 4 °C (Noiles *et al* 1995) and/or a cold shock damage or “chilling” injury during cooling (Watson 1981, Caffrey 1987, Drobnis *et al* 1993). The presence of extracellular ice further alters the cell membrane transport properties. In general, for mammalian cells the average activation energy obtained in the presence of extracellular ice is approximately twice as large as that for studies conducted in unfrozen solutions at higher temperatures (McGrath 1988) and three times as large in human granulocytes (Schwartz and Diller 1993). These changes in membrane transport properties might be associated with a variety

of thermotropic (temperature dependent) phase phenomena. For example, the temperature reduction which induces solidification in the extracellular medium may lead to lyotropic (i.e. independent of cooling rate) membrane phase changes and corresponding alterations of membrane permeability (Drobnis *et al* 1993, Steponkus 1984) and also membrane fluidity (Blok *et al* 1976). Clearly, the relative importance of temperature and the effect of extracellular ice on the predicted membrane permeability parameters ( $L_{pg}$  and  $E_{Lp}$ ) is dependent on the cell type.

### 3.5.5 Effect of CPAs on Membrane Transport Parameters

The DSC technique was used to obtain water transport data and water permeability parameters ( $L_{pg}[cpa]$  and  $E_{Lp}[cpa]$ ) of canine sperm cells in the presence of several concentrations of glycerol and dimethylsulfoxide. Although, the exact mechanism by which the presence of CPAs modifies the water permeability parameters is as yet unknown, several studies have shown that the presence of CPAs tends to reduce the membrane permeability parameters,  $L_{pg}[cpa]$  and  $E_{Lp}[cpa]$ . This is at least partially the case with the data shown in Tables 3.2 to 3.5, where an increase in the concentration of solutes in the extracellular medium is shown to reduce, although not significantly, the predicted value of reference membrane permeability of canine sperm cells. This trend is consistent with results reported in previous studies on membrane permeability parameters of ova and embryos, by Mazur (1990). Gilmore *et al* (1995) demonstrated that the value of  $L_p[cpa]$  obtained in the presence of various CPAs (1M glycerol; 1M propylene glycol; 1M dimethylsulfoxide, DMSO and 2M ethylene glycol) is lower by 30 to 60% than that obtained in their absence for human sperm cells at suprazero temperatures (i.e.  $L_p[cpa] < L_p$ ). Smith *et al* (1998) also report a similar decrease in the value  $L_{pg}[cpa]$  in isolated rat hepatocytes in the presence of 1M and 2M DMSO using standard cellular

cryomicroscopy. Mazur [42] states that  $E_{Lp}$  remains unaltered due to changes in the extracellular concentration (i.e.  $E_{Lp}[cpa] \sim E_{Lp}$ ); Gilmore et al. [25] measured an increase in the value of the  $E_a[cpa]$  for human sperm cells (i.e.  $E_a[cpa] > E_a$ ) using a Coulter counter technique; Smith *et al* (1998) found a decrease in the value of  $E_{Lp}[cpa]$  with increasing concentrations of DMSO for isolated rat hepatocytes (i.e.  $E_{Lp}[cpa] < E_{Lp}$ ). The activation energies found in this study (Tables 3.2 to 3.5) show no particular trend with an increase in the concentration of CPAs. Thus, no firm conclusions can be drawn as to the effect of CPAs on activation energies based on experimental data reported in the literature and in this study. Further studies are clearly needed.

### **3.5.6 Effect of CPAs on the Predicted Optimal Cooling Rates**

The DSC technique was also used to obtain water transport data and water permeability parameters ( $L_{pg}[cpa]$  and  $E_{Lp}[cpa]$ ) of canine sperm cells in several cryoprotective media (as shown in Tables 3.2 to 3.5). The theoretically predicted optimal cooling rate both in the presence and absence of CPAs are comparable ( $\pm 15\%$ ; ranging from 26.6 to 30.6 °C/min) with the exception of the values obtained at the highest concentration of CPA tested (6% glycerol). The theoretically predicted optimal cooling rate 9.2 °C/min in the presence of 6% glycerol is significantly lower than in its absence 26.6°C/min. This is a surprising result, as the presence of CPAs is expected to increase the ability of the cell membrane to dehydrate at faster cooling rates as shown for human and mouse sperm cell suspensions (Devireddy *et al* 1999(a), Devireddy *et al* 2000) and hepatocytes (Smith *et al* 1998). A similar decrease in the predicted optimal cooling rates in the presence of CPAs was observed in equine sperm cells (Devireddy *et al* 2002), as well. Also, a comparison of the parametric space that best fits the water transport data (as shown

in Fig. 5) shows that a much larger range of parameters “best fit” the canine sperm water transport data obtained in the presence of 6% glycerol data (Fig. 5 D) as opposed to that obtained in its absence (Fig. 5 A) and at the lower %’s of glycerol (Figs. 5B and 5C). The data obtained with the highest concentration of CPA suggests the possibility of a minimum threshold of CPA concentration below which the membrane permeability parameters (and consequently the optimal rates of freezing) of canine gametes are not affected. It is as yet unclear whether this minimum threshold of CPA concentration is universal or particular to canine sperm cells.

### 3.6 Conclusion

The water transport (volumetric shrinkage) data for canine sperm cells in the presence of extracellular ice and CPAs (glycerol and Me<sub>2</sub>SO) during freezing was obtained in this study using the DSC technique at two different cooling rates (5 and 10 °C/min). The DSC 5 and 10 °C/min water transport data in the presence and absence of CPAs was curve fitted to a model of water transport (Eqns. 15 and 16), to predict the membrane permeability parameters ( $L_{pg}$  and  $E_{Lp}$  or  $L_{pg}[cpa]$  and  $E_{Lp}[cpa]$ ). The predicted “combined best fit” permeability parameters ranged from,  $L_{pg} = 0.46 \times 10^{-15}$  to  $0.53 \times 10^{-15}$  m<sup>3</sup>/Ns (0.0027 to 0.0031 μm/min-atm) and  $E_{Lp} = 46.4$  to 56.0 kJ/mole (11.1 to 13.4 kcal/mole). The parameters obtained in this study are significantly different from the membrane permeability parameters reported in literature for mammalian sperm in the absence of extracellular ice at suprazero (and subzero) temperatures. The new parameters obtained in this study predict an optimal rate of freezing for canine sperm cells which is on the order of tens of degree C per min and is in close agreement with previously published and experimentally determined rates of optimal freezing for canine sperm cells.

## References

- Bernard, A. and Fuller, B. J., "Cryopreservation of human Oocytes: a review of current problems and perspectives", *Human Reproduction Update*, Vol. 2(3), 1996, pp.193-207.
- Bevington, P. R. and Robinson, D. K., "Data Reduction and Error Analysis for the Physical Sciences", 1992, 2nd ed., McGraw-Hill, New York.
- Blok, M. C., Van Dennen, L. M. M. and DeGier, J., "*Effect of gel to liquid crystalline phase transition on the osmotic behavior of phosphatidylcholine liposomes*", *Biochimica et Biophysica Acta*, Vol. 433, 1976, pp. 1-12.
- Caffrey, M., "*The combined and separate effects of low temperature and freezing on membrane lipid mesomorphic phase behavior: Relevance to cryobiology*", *Biochimica et Biophysica Acta*, Vol. 896, 1987, pp. 123-127.
- Cosman, M. D., Toner, M., Kandel, J. and Cravalho, E. G., "*An integrated cryomicroscopy system*", *Cryo-Letters*, Vol. 10, 1989, pp.17-38.
- Cummins, J. M. and Woodall, P. F., "*On mammalian sperm dimensions*", *Journal of Reproduction & Fertility*, Vol. 75, 1985, pp. 153-175.
- Curry, M. R., Millar, J. D. and Watson, P. F., "*Calculated optimal cooling rates for ram and human sperm cryopreservation fail to conform with empirical observations*", *Biology of Reproduction*, Vol. 51, 1994, pp. 1014-1021.
- Curry, M. R., Redding, B. J. and Watson, P. F., "*Determination of water permeability coefficient and its activation energy for rabbit spermatozoa*", *Cryobiology*, Vol.32, 1995, pp. 175-181.
- Day, S. H., Nicoll-Griffith, D. A. and Silva, J. M., "*Cryopreservation of rat and human liver slices by rapid freezing*", *Cryobiology*, Vol. 38, 1999, pp.154-159.
- Devireddy, R. V., Raha, D. and Bischof, J. C., "*Measurement of water transport during freezing in cell suspensions using a differential scanning calorimeter*", *Cryobiology*, 1998, Vol. 36, pp.124-155
- Devireddy, R. V. and Bischof, J. C., "*Measurement of water transport during freezing in mammalian liver tissue - Part II: The use of differential scanning calorimetry*", *ASME Journal of Biomechanical Engineering*, Vol. 120, 1998, pp. 559-569.
- Devireddy, R. V., Swanlund, D. J., Roberts, K. P. and Bischof, J. C., "*Sub-zero water permeability parameters of mouse spermatozoa in the presence of extracellular ice and cryoprotective agent,*", *Biology of Reproduction*, Vol. 61(3), 1999(a), pp.764-775

Devireddy, R. V., Smith, D. J. and Bischof, J. C., “*Mass transfer during freezing in rat prostate tumor tissue*”, *AIChE Journal*, Vol. 45(3), 1999(b), pp.639-654

Devireddy, R. V., Barratt, P. R., Storey, K. B. and Bischof, J. C., “*Liver freezing response of the freeze-tolerant wood frog, Rana sylvatica, in the presence and absence of glucose. I Experimental measurements*”, *Cryobiology*, Vol. 38, 1999(c), pp. 310-326.

Devireddy, R. V., Swanlund, D. J., Roberts, K. P., Pryor, J. L. and Bischof, J. C., “*The effect of extracellular ice and cryoprotective agents on the water permeability parameters of human sperm plasma membrane during freezing*”, *Human Reproduction*, Vol. 15, 2000, pp.1125-1135.

Devireddy, R. V., Coad, J. E. and Bischof, J. C., “*Microscopic and calorimetric assessment of freezing processes in uterine fibroid tissue*” *Cryobiology*, Vol. 42, 2001, pp.225-243.

Devireddy, R. V., Olin, T., Vincente, W., Troedsson, M. H. T., Bischof, J. C. and Roberts, K. P., “*Cryopreservation of equine spermatozoa: Optimal cooling rates in the presence and absence of cryoprotective agents*”, *Biology of Reproduction*, Vol. 66, 2002(a), pp.222-231.

Devireddy, R. V., Leo, J. S., Lowengrub, P. H. and Bischof, J. C., “*Measurement and numerical analysis of freezing in solutions enclosed in a small container*”, *International Journal of Heat and Mass Transfer*, Vol. 45, 2002(b), pp.1915-1931.

Devireddy, R. V. and Bischof, J. C., “*Recent Advances in Cryobiology Using Calorimetry*”, In: S. Kakac, H. Smirnov and M.R. Mila (eds.), *Low Temperature and Cryogenic Refrigeration*, 2003, Kluwer Academic Publishers, Dordrecht, The Netherlands, pp. 265-294.

Devireddy, R. V., Brooke, F., Godke, R. A. and Leibo, S. P., “*Subzero water transport characteristics of boar spermatozoa confirm observed optimal cooling rates*”, *Molecular Reproduction and Development*, Vol. 67, 2004, pp. 446-457

Diller, K. R. and Cravalho, E. G., “*A cryomicroscopy for the study of freezing and thawing process in biological systems,*” *Cryobiology*, Vol. 7, 1970, pp.191-199.

Drobnis, E. Z., Crowe, L. M., Berger, T., Anchoroguy, T. J., Overstreet, J. W. and Crowe, J. H., “*Cold shock damage is due to lipid phase transitions in cell membranes: a demonstration using sperm as a model*”, *Journal of Experimental Zoology*, Vol. 265, 1993, pp. 432-437.

Dobrinski, I., Lulai, C., Barth, A. D. and Post, K., “*Effects of four different extenders and three different freezing rates on post-thaw viability of dog semen*”, *Journal of Reproduction & Fertility*, Vol. 47 (Suppl.), 1993, pp. 291–296.

Diller, K. R., “*Quantitative low temperature optical microscopy of biological systems,*” *Journal of Microscopy*, Vol. 126, 1982, pp.9-28.

Du, J., Tao, J., Kleinhans, F. W., Mazur, P. and Critser, J. K., “*Water volume and osmotic behavior of mouse spermatozoa determined by electron paramagnetic resonance*”, *Journal of Reproduction & Fertility*, Vol. 101, 1994, pp.37-42.

England, G. C. W., “*Cryopreservation of dog semen: A review*”, *Journal of Reproduction & Fertility*, Vol. 47 (Suppl.), 1993, pp. 243– 255.

Fontbonne, A., and Badinand, F., “*Canine artificial insemination with frozen semen: Comparison of intravaginal and intrauterine deposition of semen*”, *Journal of Reproduction & Fertility*, Vol. 47 (Suppl.), 1993, pp. 325–327.

Foote, R. H., “*The effects of electrolytes, sugars, glycerol, and catalase on survival of dog sperm stored in buffered-yolk mediums*”, *American Journal of Veterinary Research*, Vol. 25, 1964, pp. 32–36.

Gao, D. Y., Liu, J., Liu, C., McGann, L. E., Watson, P. F., Kleinhans, F. W., Mazur, P., Critser, E. S. and Critser, J. K., “*Prevention of osmotic injury to human spermatazoa during addition and removal of glycerol*”, *Human Reproduction*, Vol. 10, 1995, pp. 1109-1122.

Gao, D. Y., Mazur, P. and Critser, J. K., “*Fundamental cryobiology of mammalian spermatozoa*”. In: A. M. Karow, J. K. Critser (eds.), 1997, *Reproductive Tissue Banking*, pp. 263-328.

Garner, G. L., Johnson, L. A., Yue, S. T. and Roth, B. L., “*Dual DNA staining assessment of bovine sperm viability using SYBR-14 and propidium iodide*”, *Journal of Andrology*, Vol. 15, 1994, pp. 620-629.

Garner, G. L. and Johnson, L. A., “*Viability assessment of mammalian sperm using SYBR-14 and propidium iodide*”, *Biology of Reproduction*, vol. 53, 1995, pp. 276–284.

Gilmore, J. A., McGann, L. E., Liu, J., Gao, D. Y., Peter, A. T., Kleinhans, F. W. and Critser, J. K., “*Effect of cryoprotectant solutes on water permeability of human spermatozoa*”, *Biology of Reproduction*, Vol. 53, 1995, pp. 985-995.

Gilmore, J. A., Du, J., Tao, J., Peter, A. T. and Critser, J. K., “*Osmotic properties of boar spermatozoa and their relevance to cryopreservation*”, *Journal of Reproduction & Fertility*, Vol. 107, 1996, pp. 87–95.

Gilmore, J. A., Liu, J., Peter, A. T. and Critser, J. K., “*Determination of plasma membrane characteristics of boar spermatozoa and their relevance to cryopreservation*”, *Biology of Reproduction*, Vol. 58, 1998, pp. 28–36.

Hansel, W. and McEntee, K., “*Male reproductive process*”, in: M. J. Swenson (Ed.) 1970, *Duke’s physiology of domestic animals*, 8<sup>th</sup> ed., Cornell Univ. Press, Ithaca and London, pp. 1298-1338.

Hay, M. A., King, W. A., Gartley, C. J., Leibo, S. P. and Goodrowe, K. L., “*Canine spermatozoa — Cryopreservation and evaluation of gamete interaction*”, *Theriogenology*, Vol. 48, 1997, pp. 1329–1342.

Gray, A., “*Analytical Calorimetry*,” 1976, Plenum Press, New York, pp. 322

Harris, C. L., Toner, M., Hubel, A., Cravalho, E. G., Yarmush, M. L. and Tompkins, R. G., “*Cryopreservation of isolated hepatocytes: Intracellular ice formation under various chemical and physical conditions*,” *Cryobiology*, Vol.28, 1991, pp.436-444.

Henry, M. A., Noiles, E. E. Gao, D., Mazur, P. and Critser, J. K., “*Cryopreservation of human spermatozoa. IV. The effects of cooling and warming rate on the maintenance of motility, plasma membrane integrity, and mitochondrial function*,” *Fertility and Sterility*, Vol. 60, 1993, pp. 911-918.

Hubel, A., Toner, M., Cravalho, E. G., Yarmush, M. L. and Tompkins, R. G., “*Intracellular ice formation during the freezing of hepatocytes cultured in a double collagen gel*,” *Biotechnology Progress*, Vol. 7, 1991, pp.554-559.

Ishiguro, H. and Rubinsky, B., “*Mechanical interaction between ice crystals and red blood cells during directional solidification*,” *Cryobiology*, Vol. 31, 1994, pp.483-500.

Karlsson, J. O., Cravalho, E. G., Borel, R. I., Tompkins, R. G., Yarmush, M. L., and Toner, M., “*Nucleation and growth of ice crystals inside cultured hepatocytes during freezing in the presence of dimethylsulfoxide*”, *Biophysics Journal*, Vol. 65, 1993, pp. 2524-2536.

Karlsson, J. O., Cravalho, E. G. and Toner, M., “*A model of diffusion-limited ice growth inside biological cells during freezing*”, *Journal of Applied Physics*, Vol. 75, 1994 pp. 4442-4455.

Kedem, O. and Katchalsky, A., “*Thermodynamic analysis of the permeability of biological membranes to non-electrolytes*”, *Biochimica et Biophysica Acta*, Vol. 27, 1958, pp. 229-246.

Kleinhans, F. W., Travis, V. S., Du, J., Villines, P. M., Colvin, K. E. and Critser, J. K., “*Measurement of human sperm intracellular water volume by electron spin resonance*”, *Journal of Andrology*, Vol. 13, 1992, pp. 498-506.

Leibo, S.P., “*Water permeability and its activation energy of fertilized and unfertilized mouse ova*,” *Journal of Membrane Biology*, Vol.53, 1980, pp.179-188.

Levin, R. L., Cravalho, E. G. and Huggins, C.G., “*A membrane model describing the effect of temperature on water conductivity of erythrocyte membranes at subzero temperatures*,” *Cryobiology*, Vol. 13, 1976, pp.415-429.

Levin, R. L., Cravalho, E. G. and Huggins, C.G., “*Effect of solution non-ideality on erythrocytes volume regulation*,” *Biochimica et Biophysica Acta*, Vol. 465, 1977, pp. 179-190.

Levin, R. L., Ushiyama, M. and Cravalho, E. G., “*Water permeability of yeast cells at sub-zero temperatures*,” *Journal of Membrane Biology*, Vol. 46, 1979, pp. 91-124.

Linde-Forsberg, C. and Forsberg, M., “*Fertility in dogs in relation to semen quality and the time and site of insemination with fresh and frozen semen*”, *Journal of Reproduction & Fertility*, Vol. 39 (Suppl.), 1989, pp. 299–310.

Linde-Forsberg, C., Ström Holst, B. and Govette, G., “*Comparison of fertility data from vaginal vs intrauterine insemination of frozen–thawed dog semen: A retrospective study*”, *Theriogenology*, Vol. 52, 1999, pp. 11–23.

Lovelock, J. E., “*Haemolysis of human red blood cells by freezing and thawing*,” *Biochimica et Biophysica Acta*, Vol. 10, 1953, pp.414-426.

Mansoori, G. A., “*Kinetics of water loss from cells at subzero centigrade temperatures*,” *Cryobiology*, Vol. 12, 1975, pp.34-45.

Mazur, P., “*Kinetics of water loss from cells at subzero temperatures and the likelihood of intracellular freezing*,” *Journal of General Physiology*, Vol. 47, 1963, pp.347-369.

Mazur, P., “*Cryobiology: The freezing of biological systems*,” *Science*, Vol. 168, 1970, pp.939-949.

Mazur, P., Leibo, S. P. and Chu, E. H. Y., “*A two-factor hypothesis of freezing injury*,” *Experimental Cell Research*, Vol. 71, 1972, pp.345-355.

Mazur, P., “*Freezing of living cells: Mechanisms and implications*,” *American Journal of Physiology*, Vol. 247, 1984, pp. C125-C142

Mazur, P., “*Equilibrium, quasi-equilibrium, and nonequilibrium freezing of mammalian embryos*”, *Cell Biophysics*. Vol. 17, 1990, pp. 53-92.

McCaa, C., Diller, K. R., Aggarawal, S. J. and Takahashi, T., “*Cryomicroscopic determination of the membrane osmotic properties of human monocytes at subfreezing temperatures*”, *Cryobiology*, Vol. 28, 1991, pp. 391-399.

McGrath, J. J., Cravalho, E. G. and Huggins, C. E., “*An experimental comparison of intracellular ice formation and freeze thaw survival of HeLa S-3 cells*” ,*Cryobiology*, Vol. 12, 1975, pp. 540-550

McGrath, J. J., “*Preservation of biological material by freezing and thawing*”, *Heat transfer in medicine and biology*, A. Shitzer and R.C Eberhart (eds.), 1985, Plenum Press., New York

McGrath, J. J., “*Membrane transport properties*”. In: McGrath, J. J., Diller, K.R (eds.), *Low temperature biotechnology: Emerging applications and engineering contributions*, 1988, BED - Vol. 10, HTD -Vol. 98, ASME Press, pp.273-330

McNaughton, J. L. and Mortimer C. T., “*Differential Scanning Calorimetry*”, 1975, Perkin-Elmer, Norwalk

Molish, H., “*Untersuchen uber das erfieren der pflanzen*”, Fisher, Jena, Reprinted in English 1982 in *Cryo-Letters*, Vol. 3, 1897, pp.332-390

Montgomery, D. C. and Runger, G. C., “*Applied Statistics and Probability for Engineers*”, 1994, John Wiley & Sons, Inc., New York, pp. 471-529.

Noiles, E. E. Mazur, P. Watson, P. F., Kleinhans, P. F. and Critser, J. K., “*Determination of water permeability coefficient for human spermatozoa and its activation energy*”, *Biology of Reproduction*, Vol. 48, 1993, pp. 99-109.

Noiles, E. E., Bailey, J. L., B. T. Storey B. T., “*The temperature dependence in the hydraulic conductivity,  $L_p$ , of the mouse sperm plasma membrane shows a discontinuity between 4 and 0 degrees °C*”, *Cryobiology*, Vol. 32, 1995, pp. 220-238.

Oegema, T. R., Deloria, L. B., Fedewa, M., Bischof, J. C. and Lewis, J. L., “*A simple cryopreservation method for the maintenance of cell viability and mechanical integrity of cultured cartilage analog*”, *Cryobiology*, Vol. 40, 1999, pp.370-375

Ostrander, E. A., Galibert, F. and Patterson, D. F., “*Canine genetics comes of age*”, *Trends Genet.* 16 (2000)117-124.

Ostrander, E. A. and Kruglyak, L., “*Unleashing the canine genome*”, *Genome Res.* 10 (2000) 1271-1274.

Pazhayannur, P. V. and Bischof, J. C., “*Measurement and simulation of water transport during freezing in mammalian liver tissue*”, *ASME Journal of Biomechanical Engineering*, Vol.119, 1997, pp. 269-277

Pinto, C. R. F., Paccamonti, D. L. and Eilts, B. E., “*Fertility in bitches artificially inseminated with extended, chilled semen*”, *Theriogenology*, Vol. 52, 1999, pp. 609–616.

Rodriguez-Martinez, J. H., Ekwall, H. and Linde-Forsberg, C., “*Fine structure and elemental composition of fresh and frozen dog spermatozoa*”, *Journal of Reproduction & Fertility*, Vol. 47, 1993, pp. 279–285.

Rota, A., Peña, A. I. Linde-Forsberg, C. and Rodriguez-Martinez, H., “*In vitro capacitation of fresh, chilled and frozen-thawed dog spermatozoa assessed by chlortetracycline assay and changes in motility patterns*”, *Animal Reproduction Science*, Vol. 57, 1999, pp. 199–215.

Scheiwe, M. W. and Korber, C., “*Thermally defined cryomicroscopy and thermodynamic analysis in lymphocyte freezing*”, *Cryobiology*, Vol. 21, 1984, pp. 93-105

Schwartz, G. J. and Diller, K. R., “*Volumetric changes during thawing of frozen cells*”, *Cryo-Letters*, Vol.1, 1980, pp.338-354

Schwartz, G. J. and Diller, K. R., “*Analysis of the water permeability of human granulocytes at subzero temperatures in the presence of extracellular ice*”, *ASME Journal of Biomechanical Engineering*, Vol. 105, 1993, pp. 360-366

Silva, L. D. M., Onclin, K., Lejeune, B. and Verstegen, J. P., “*Comparison of intravaginal and intrauterine insemination of bitches with fresh or frozen semen*”, *Veterinary Record*, Vol. 138, 1996, pp.154–157.

Smith, D. J., Josephson, S. J. and Bischof, J. C., “*A model of cryosurgical destruction in AT-1 prostate tumor based on cellular damage mechanisms*”, In: S. Clegg (ed.), *Advances in Heat and Mass Transfer in Biotechnology*, 1997, Plenum Press, New York, BED-Vol. 37. HTD-Vol. 355, pp. 149-150.

Smith, D. J., Schulte, M. and Bischof, J. C., “*The effect of dimethylsulfoxide on the water transport response of rat hepatocytes during freezing*”, *ASME Journal of Biomechanical Engineering*, Vol. 120, 1998, pp.549-558.

Steponkus, P. L., “*Role of the plasma membrane in freezing injury and cold acclimation*”, *Annual Review of Plant Physiology*, Vol. 35, 1984, pp. 543-584.

Steponkus, P. L., Dowgert, M. F., Ferguson, J. R. and Levin, R. L., “*Cryomicroscopy of isolated plant protoplasts*”, *Cryobiology*, Vol. 20, 1983, pp. 1138-1162

Toner, M., Cravalho, E. G. and Armant, D. R., “*Water transport and estimated transmembrane potential during freezing of mouse oocytes*”, *Journal of Membrane Biology*, Vol. 115, 1990, pp. 261-272.

Toner, M., Cravalho, E. G. and Karel, M., “*Thermodynamics and kinetics of intracellular ice formation during freezing of biological cells*”, *Journal of Applied Physics*, Vol. 10, 1991, pp. 463-465

Toner, M., Tompkins, R. G., Cravalho, E. G. and Yarmush, M. L., “*Transport phenomena during freezing of isolated hepatocytes*”, *AIChE Journal*, Vol. 38, 1992, pp. 1512-1522.

Toner, M., “*Nucleation of ice crystals in biological cells*” In: P. L. Steponkus (ed.), 1993, *Advances in low-temperature biology*, Vol. 2, JAI Press, pp. 1-52.

Thirumala, S., Ferrer, M. S., Al-Jarrah, A., Eilts, B. E., Paccamonti, D. L. and Devireddy, R. V., “*Cryopreservation of canine spermatozoa: theoretical prediction of optimal cooling rates in the presence and absence of cryoprotective agents*”, *Cryobiology*, Vol. 47, 2003, pp. 109-124

Walsh, J. R., “*Modeling and design of algal cryopreservation protocols*”, Ph.D. Dissertation, The University of Texas at Austin, Austin, Texas.

Watson, P. F., “*The effects of cold shock on sperm cell membranes*”. In: G. J. Morris, A. Clarke (eds.), 1981, *Effects of low temperature on biological membranes*, Academic Press, London, UK, pp. 189-218.

Yu, I., Songsasen, N., Godke, R. A. and Leibo, S. P., “*Differences among dogs in responses of their spermatozoa cryopreserved at various cooling and warming rates*”, *Cryobiology*, Vol. 44, 2002, pp.57–72.

## **Vita**

Sreedhar Thirumala is from a small town, Amerchintha in India. He got his primary and secondary education from Government High School in Amerchintha. He received his Diploma in Mechanical Engineering from Government Polytechnic College, Mahabub Nager, India, in 1995. He received the degree of Bachelor of Technology in Mechanical Engineering from Jawaharlal Nehru Technological University, Hyderabad, India, in 2000. After his graduation, he worked as a Product Engineer in SIDRA Castings Pvt. Limited., Hyderabad, India, a small engineering industry involved in the design, manufacture, and supply of roller bearings till November, 2001. He then joined the graduate program at Louisiana State University, Baton Rouge (LSU) in January, 2002. He is a candidate for the degree of Master of Science in Mechanical Engineering to be awarded at the commencement of May, 2004. After completing his master's degree he would be pursuing his doctoral program.